### Title

Printing Multi-Material Organic Haptic Actuators




### Journal

Advanced Materials, 33(19)

### ISSN

0935-9648



### Authors

Zhai, Yichen

Wang, Zhijian

Kwon, Kye-Si

et al.



### Publication Date

2021-05-01

### DOI

10.1002/adma.202002541

Peer reviewed

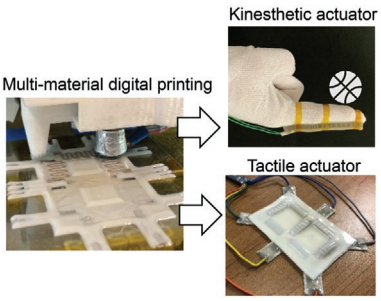


An overview of emerging organic actuator materials and digital printing technologies for fabricating soft organic haptic actuators to emulate touch sensations is provided. In particular, the focus is on the challenges and potential solutions associated with integration of multi-material actuators. The progress in achieving compact, lightweight haptic actuators by combining different polymers and composites in freeform designs is reported.

ADVANCED MATERIALS
www.advmat.de

# Printing Multi-Material Organic Haptic Actuators

*Yichen Zhai, Zhijian Wang, Kye-Si Kwon, Shengqiang Cai, Darren J. Lipomi, and Tse Nga Ng**

**Haptic actuators generate touch sensations and provide realism and depth in human–machine interactions. A new generation of soft haptic interfaces is desired to produce the distributed signals over large areas that are required to mimic natural touch interactions. One promising approach is to combine the advantages of organic actuator materials and additive printing technologies. This powerful combination can lead to devices that are ergonomic, readily customizable, and economical for researchers to explore potential benefits and create new haptic applications. Here, an overview of emerging organic actuator materials and digital printing technologies for fabricating haptic actuators is provided. In particular, the focus is on the challenges and potential solutions associated with integration of multi-material actuators, with an eye toward improving the fidelity and robustness of the printing process. Then the progress in achieving compact, lightweight haptic actuators by using an open-source extrusion printer to integrate different polymers and composites in freeform designs is reported. Two haptic interfaces—a tactile surface and a kinesthetic glove—are demonstrated to show that printing with organic materials is a versatile approach for rapid prototyping of various types of haptic devices.**

## 1. Introduction

Haptic technologies interact with users through the sense of touch, generating sensations to help people in manipulation tasks and provide information of their surroundings in virtual or augmented reality.[1–5] Haptic systems that can realistically recreate touch sensations will greatly impact our professional and personal lives in many areas including teleoperation, simulation training, communication, and immersive entertainment. Yet, the utility of haptics is currently limited; moreover, it is challenging to produce the large-area, distributed signals required to mimic natural touch.

It would be desirable for haptic actuators to generate large ranges of forces and displacements over short time scales, in a compact form factor in the case of wearable haptics. This dynamism is required because the structures such as the skin and elements of the musculoskeletal system are highly stretchable. Moreover, they are teeming with mechanosensory neurons that can perceive sub-micron surface features and macroscale displacements, with reaction times in milliseconds.[3,5] Thus, to accommodate this dynamism and sensitivity, an exceptionally versatile suite of materials and tools is required to realize the entire range of haptic perception.

Haptic perception can be divided into two parts: the tactile and kinesthetic senses.[6–8] The tactile sense involves the nerve endings in the skin to detect contact, texture, and vibration. The kinesthetic sense is the awareness of the body position and involves structures located in the musculoskeletal system to sense force and motion. For example, to emulate the feeling of grasping a cup, a haptic system would need to trigger both tactile and kinesthetic senses. That is, pressure would be applied on the fingers to indicate contact, and other actuators located at the joints of the fingers would stiffen to produce resistance against moving into the space occupied by the cup. In comparison to visual or auditory inputs aiming at localized organs of eyes and ears, haptic systems require distributed inputs covering the body. The complexity involved to simulate haptic signals over large area, with sufficient spatial and temporal resolution and high dynamic range, has been a considerable challenge and thus presents exciting research opportunities.

Conventional micro-electromechanical system (MEMS) has been used to implement vibrational feedback, which is the most common type of haptic effect in commercial devices today. However, fabrication techniques for MEMS are catered toward micrometer length scales and hence research is still needed to scale up MEMS assembly[9,10] for large, customized human interfaces. To realize many other promising haptic modalities, new materials and processing technologies are being explored to make devices that improve haptic realism and scalability for mass manufacturing.

Y. Zhai, Prof. T. N. Ng
Department of Electrical and Computer Engineering
University of California San Diego
9500 Gilman Dr., La Jolla, CA 92093, USA
E-mail: tnn046@ucsd.edu
Dr. Z. Wang, Prof. S. Cai
Department of Mechanical and Aerospace Engineering
University of California San Diego
9500 Gilman Dr., La Jolla, CA 92093, USA
Prof. K.-S. Kwon
Department of Mechanical Engineering
Soonchunhyang University
Asan City, Chungnam 31538, South Korea
Prof. D. J. Lipomi
Department of Nanoengineering
University of California San Diego
9500 Gilman Dr., La Jolla, CA 92093, USA
The ORCID identification number(s) for the author(s) of this article can be found under https://doi.org/10.1002/adma.202002541.

**DOI: 10.1002/adma.202002541**

 

Herein, we will present the latest advancements in the development of organic actuators, namely, polymeric structures that change their mechanical properties with stimuli. Organic actuators are capable of large actuation strain (10–50%) and high energy output per weight unit, to complement rigid ceramic actuators that output high stress but low actuation strain (<0.1%).[11–13] Many organic materials are flexible, lightweight, and conformable, with characteristics particularly suitable for mimicking touch interactions with soft biological bodies and ensuring ergonomics and portability of wearable haptics. The wide diversity of molecular structures and organic composites allow precise fine-tuning of various properties including surface adhesion and friction, texture, and viscoelasticity to expand the repertoire of haptic systems. In addition, polymers and organic composites are easily processable by low-cost techniques, such as extrusion, molding, and lamination, which can be applied to large areas with high throughput. The compatibility of organics with additive printing techniques[14–17] enables further customization and rapid prototyping of personalized haptic devices.

Emerging additive manufacturing techniques such as digital printing provide the capability to fabricate multi-scale, multi-material designs with high precision and throughput. In an actuator, multiple materials are required to connect mechanical and electronic function. For instance, electrical conductors are incorporated with the mechanical structure, in order to apply stimuli such as voltage or heat to trigger actuation. Digital printing is amenable for integrating multiple materials and architecting functionally gradient materials to increase the design space for versatile motion.[18,19] Moreover, printers can be coordinated with pick-and-place tools[20–22] to add silicon chips for programmable electronic control within the haptic device. The versatility and reconfigurability of printing processes are advantageous for fabricating integrated organic haptic interfaces, as will be showcased in this report.

To familiarize our readers with haptic technologies, we provide an overview of recent innovations in Section 2. We then turn our focus to printable organic haptic devices. The main categories of organic actuators—including the associated materials and working mechanisms—are surveyed in Section 3. The choices of digital printing methods to fabricate organic actuators are presented in Section 4, followed by a discussion on integration challenges and potential solutions with regard to printing multi-material actuators in Section 5. In Section 6, we present our progress with two demonstrations: i) a compact tactile surface and ii) a lightweight kinesthetic glove, both of which are electrically programmable, without the need of heavy auxiliary equipment like air compressors required for pneumatic devices. These proof-of-concept devices were fabricated by printing liquid crystal elastomer as the material used for actuation, along with soft electrical conductors[23,24] and other non-actuated structural components. We found that our approach was able to afford a form factor that is more conformal and portable than prior demonstrations. In Section 7, we conclude with our opinions on the future prospects of organic haptic technologies.

## 2. Overview of Haptic Technologies

Haptics is the study of human touch perception; it is a broad field at the nexus of cognitive science and multiple branches of applied science (including mechanical and electrical engineering and materials science). Its goal is to advance technologies to create mechanical, thermal, and electrically transduced sensations. The recent report[4] by Lipomi et al. explains integrative approaches to bridge materials science and psychology to better understand haptic perception. And the review by Biswas and Visell[3] includes descriptions of materials-based technologies amenable to a future "haptic display," along with an excellent tutorial on the anatomy and mechanisms of tactile receptors. To recapitulate the main points for our readers, skin is the largest organ of the body, categorized into hairy skin that covers most of the body surface and glabrous (hairless) skin on the palmer surface hands and feet with higher density of mechanoreceptors than in hairy skin. The mechanoreceptors and nociceptors in glabrous skin capture information about thermal, mechanical, and noxious (itchy/painful) stimuli from the environment. The corpuscles are innervated by sensory neurons, which in turn transmit encoding spikes to the brain to indicate the touch location, intensity, and timing for tactile perception. For kinesthetic sensations, the afferent or sensory neurons in muscles and connective tissues are triggered by movement and physical forces, to generate a dynamic sense of one's own body positions and exertions. Since haptic perception encompasses the two modalities of tactile and kinesthetic senses, the goal of haptic technologies is to incorporate actuators that reproduce the "feel" of surface properties and bulk resistance as expected from touch interactions.

While the most common haptic technology is the vibrational feedback from mobile devices in consumer electronics, there is high demand for additional techniques to provide sensations at surfaces. Other modes to produce tactile sensations for touch screens involve changing the surface friction,[25] adhesion,[30] temperature,[31] viscoelasticity,[32] and morphology[33–35] at the skin–screen interface. As illustrated in **Figure 1**a, the electrostatic friction between a moving finger and an encapsulated electrode can be tuned by applying voltage at different frequencies and amplitudes, leading the user to perceive the device surface varying between sticky versus slippery, bumpy versus smooth, and so forth.[25] To demonstrate a Braille display for the visually impaired, tactile pixel arrays were designed[26] as in Figure 1b to form letter cells by locally lifting up dots and changing the morphology of flexible surfaces. Most haptic devices are targeted to interact with our hands, but it will be more immersive to expand touch feedback to more areas of the body. In this vein, the form factor of surface haptics has been recently extended to wearable sheets[2] in Figure 1c, with magnetic coil actuators that conform to the body.

In addition to mimicking tactile sensations, haptic systems can also deliver kinesthetic feedback. In such systems, perceived resistance is adjusted to emulate the solidness of objects in virtual reality. For example, a combination of motors or hydraulic/pneumatic actuators can be fitted to an exoskeleton to apply force feedback in Figure 1d. The force and torque exerted by the haptic gripper[27] in Figure 1e trigger kinesthetic and vibrotactile sensations to assist in robotic manipulation tasks. Haptic devices on fingertips[28] in Figure 1f convey forces by deforming

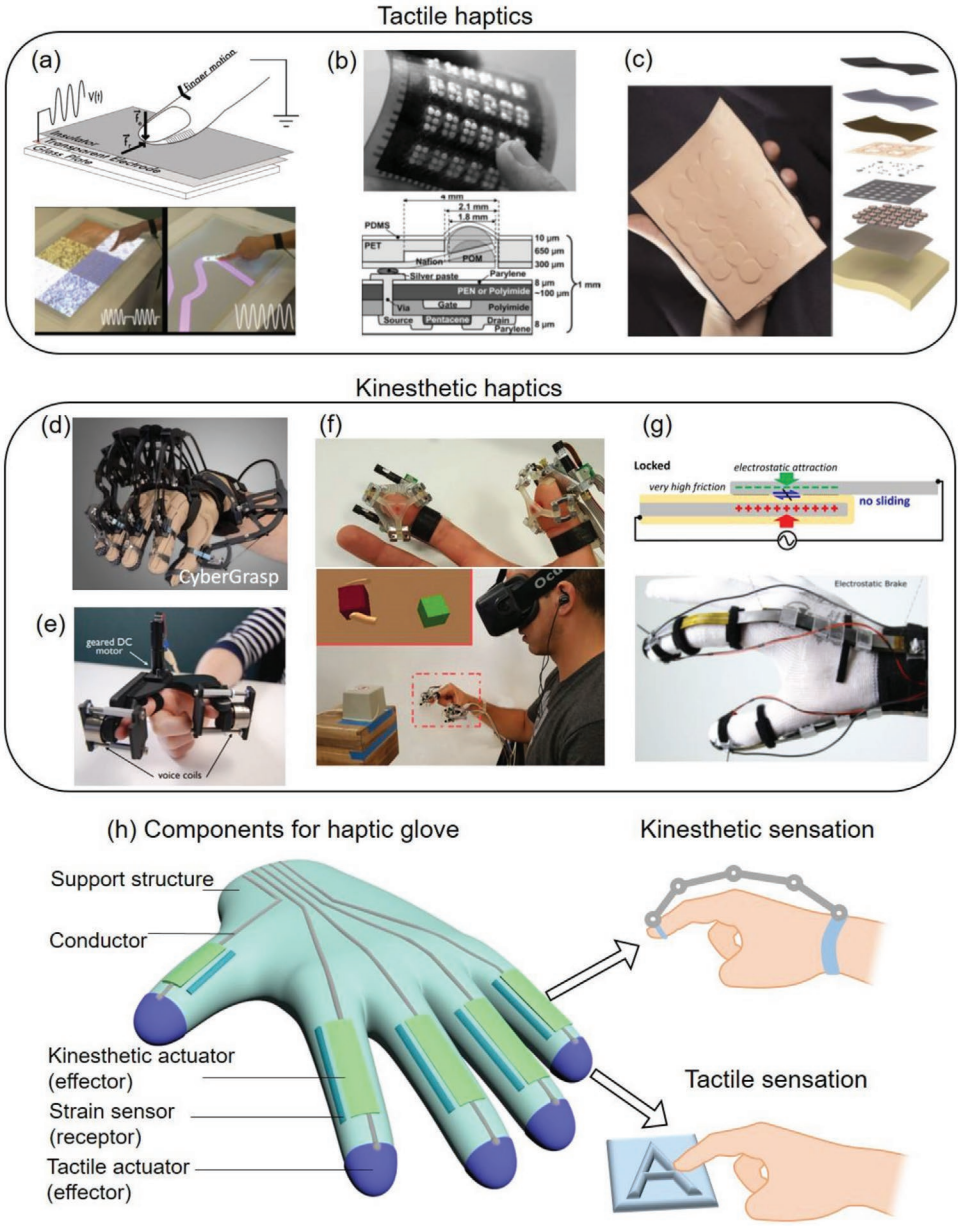


**Figure 1.** a) Electrovibration tactile surface. b) Braille tactile display. c) Skin-integrated wireless tactile interface for mechanical vibration feedback. d) Commercial haptic feedback system CyberGrasp. e) Gripper controller with haptic feedback. f) Virtual object manipulation and exploration based on fingertip actuators driven by motors. g) Conformal electrostatic clutches providing kinesthetic feedback. h) Concept of a compact haptic feedback glove. a) Reproduced with permission.[25] Copyright 2010, ACM. b) Reproduced with permission.[26] Copyright 2007, IEEE. c) Reproduced with permission.[2] Copyright 2019, Springer Nature. d) Photo reproduced with permission from CyberGlove Systems. http://www.cyberglovesystems.com/. e) Reproduced with permission.[27] Copyright 2014, IEEE. f) Reproduced with permission.[28] Copyright 2017, ACM. g) Reproduced with permission.[29] Copyright 2018, ACM.

skin to simulate objects with different mass, friction, and stiffness. Devices incorporating an exoskeleton[36–38] can provide the mechanical support for enabling fast and powerful haptic feedback, but structures of such bulk can limit portability and comfort. To reduce the size, weight, and power requirements, new concepts are being developed to demonstrate lightweight, soft actuators capable of providing kinesthetic feedback.[29,39] For example, Figure 1g shows a fabric glove instrumented with thin strips of sliding electrostatic clutches that are capable of generating locking forces on finger joints.[29]

A compact haptic glove with coordinated tactile and kinesthetic actuators, as depicted in Figure 1h, will improve user mobility and experience, making haptic interfaces more effective in rehabilitation,[40,41] training,[42] teleoperation,[43] and navigation controls.[44] There is close connection between haptics and the field of soft robotics.[45–48] With the increase in the use of robotics for remote environments, electronic skins[49–53] based on flexible organic sensors are being developed for robots to sense the environment. The next extension is to enable bidirectional communications between robots and users, to

convey the sensory stimuli gathered by robots to people as haptic feedback. Organic polymers with mechanical responses inspired by muscle are attractive as materials that can safely and unobtrusively interface with humans. The potential of a soft polymer actuator to match the stiffness of biological tissue is an advantage in medical applications. In the next section, we introduce organic actuators. In particular, we discuss several types of materials and operating principles which allow them to generate mechanical forces sufficiently high for human perception.

## 3. Materials and Mechanisms of Organic Actuators

In haptic applications, the metrics to evaluate actuator performance[54–56] include blocking stress and active strain. **Figure 2**a compares these two metrics for different classes of actuator materials.[57] The blocking stress is defined as the stress generated by the material against the constraint (zero deformation) when it is actuated. The active strain is often measured as the deformation of a material in a free standing state during actuation. The dashed lines in Figure 2a indicate constant values of stiffness, which is the ratio of the blocking stress to active strain. The stiffness of an actuator can be matched to human tissues to improve comfort and ergonomics. The gray area in Figure 2a marks the region characteristic of human muscles. Inorganic materials such as piezoelectric ceramics and shape memory metal alloys show stress–strain characteristics in the upper left region of Figure 2a, exhibiting high stress but low strain typically less than 0.1%, which is too low for humans to perceive. Soft organic materials, such as liquid crystal elastomers and magnetic composites, are in the lower right region with high output strain and relatively low actuating stress, making them suitable for haptic applications. Below we will introduce major classes of soft organic actuators,[58] categorized according to their actuation mechanisms.

### 3.1. Swelling Driven Hydrogels

As depicted in Figure 2b, hydrogels absorb water and show dramatic changes in volume when the balance between the elasticity of polymer chain and the osmosis shifts with external stimuli.[66,67] The volume change is dependent on the crosslinking density, which can be precisely controlled by adjusting the material composition and processing method. The structural changes between dry and swollen states can be adjusted by varying parameters such as pH, solute molarity, and temperature, and are predictable by simulations. In order to achieve anisotropic swelling, hydrogels consisting of aligned cellulose fibrils embedded in a soft acrylamide matrix are obtained by extrusion.[68] The resulting composite swells less along the longitudinal axis than the transverse axis perpendicular to the fibrils. The shape change with anisotropic swelling can be designed through solving the inverse problem for the target geometries.[68] The limitation with hydrogel actuators is that their response speed is often slow, because they rely on diffusion to switch between swollen and shrunken states.

### 3.2. Thermally Driven Polymers

Thermally driven polymers include shape memory polymers (SMPs), liquid crystal elastomers (LCEs), and thermal expansion polymers. These materials actuate when the temperature is raised by joule heating or illumination.[69] SMPs are polymers such as polyurethane and polycaprolactone with permanent and temporary networks.[62,70,71] As shown in Figure 2c, the temporary network can be disconnected at an elevated temperature. Once disconnected, the materials are deformed and held in the temporary position and cooled down below the transition temperature, in order to fix the temporary shape. Then when heat is applied again, the object shape will revert back to the initial shape, due to the stored elastic energy in the polymer network. The shape change in SMP is often a one-time event, acceptable for applications like the expansion of cardiovascular stents. On the other hand, to enable reversible actuation, the use of LCE allows cycling between deformation states. Thermal expansion polymers utilize the thermal expansion of material to generate mechanical actuation.[72–74] They can be used to fabricate micro structures in high resolution. The actuation of such materials is reversible, yet the deformation strain is often lower compared to SMPs and LCEs.

LCEs are polymers that switch from liquid-crystal phase to isotropic phase upon heating, resulting in large contraction in the alignment direction as illustrated in Figure 2d. The deformation of a LCE actuator depends on the alignment direction and structure of the liquid crystal mesogens. The mesogens are aligned by mechanical stretching, electromagnetic field, or shear extrusion.[75–81] For thermally driven polymers, the time to reach the isotropic phase with heating is on the order of tens of seconds; but to revert back to the liquid-crystal phase, the speed can be slower, depending on the rate of heat flow from the actuator to the environment.

### 3.3. Magnetic Composites

Another type of polymeric actuator of interest for haptics is a magnetic composite,[64,82–84] in which magnetic particles are embedded in an elastomeric matrix. In response to an external magnetic field, the magnetic domains rotate and generate micro-torque, leading to macroscopic mechanical deformation, as shown in Figure 2e, and magnetic actuators have demonstrated multiple modes of actuation. The magnetic composites can be processed by extrusion, in which an electric coil attached to the nozzle is programmed to generate a tunable magnetic field to align the magnetic particles in the desired orientation. The function and performance of magnetic composite actuators are influenced by choices of magnetic particles with different coercivity fields and remnant magnetizations, particle loading densities, and matrix materials.[85] Magnetic composite actuators show a fast response time of tens of milliseconds.

### 3.4. Electroactive Polymers

Electroactive polymers (EAPs) exhibit deformation upon the application of a voltage. Actuators based on EAPs require

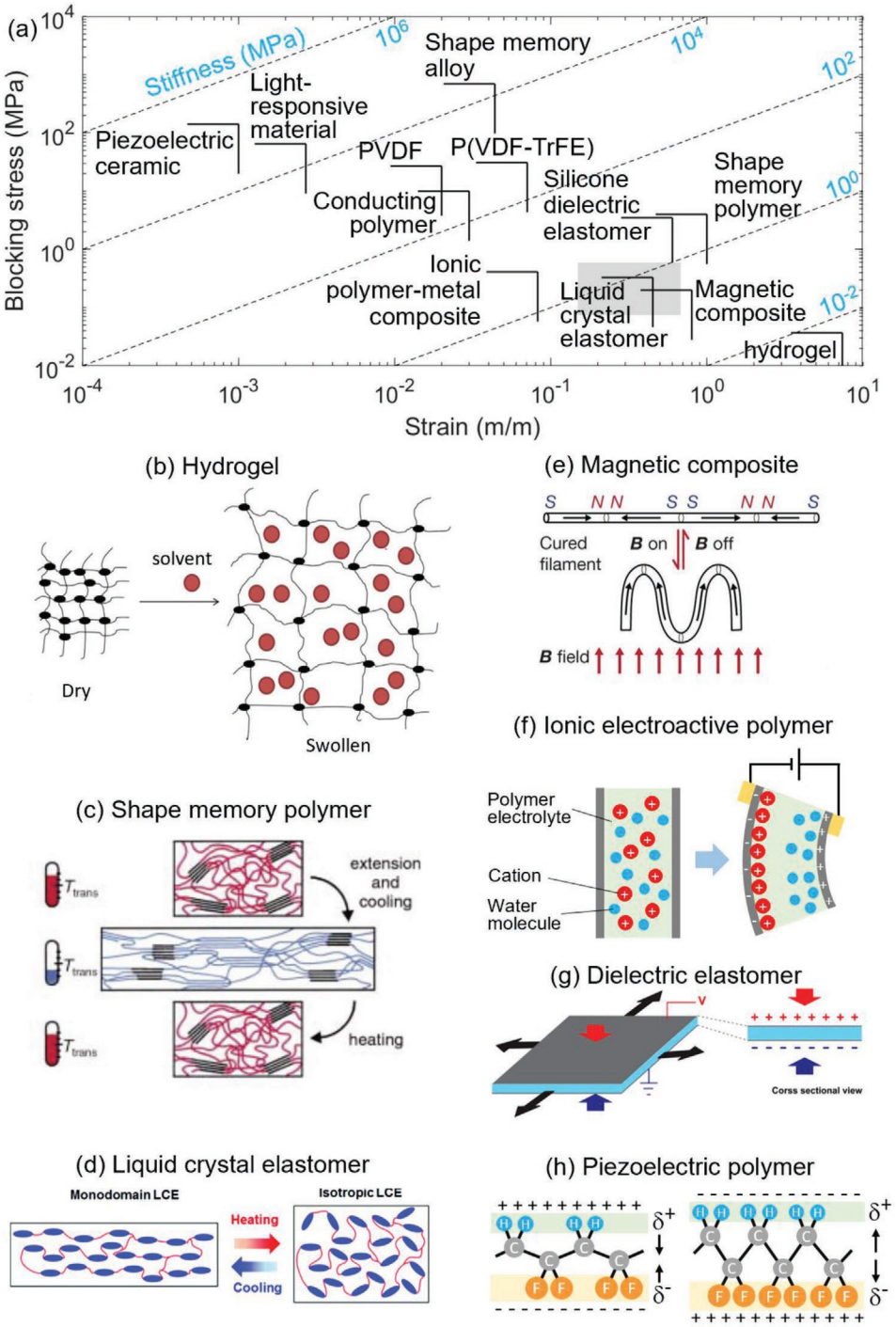


**Figure 2.** a) Range of blocking stress and actuation strain for various actuator materials. The values are from refs. [57,59,60]. Schematics illustrating the operational mechanisms for organic actuators based on: b) hydrogel; c) shape memory polymer; d) liquid-crystal elastomer; e) magnetic composite; f) ionic electroactive polymer; g) dielectric elastomer. h) Piezoelectric polymer. b) Adapted with permission.[61] Copyright 2016, IWA Publishing. c) Reproduced with permission.[62] Copyright 2002, Wiley-VCH. d) Reproduced with permission.[63] Copyright 2017, RSC Publishing. e) Reproduced with permission.[64] Copyright 2018, Springer Nature. g) Reproduced with permission.[65] Copyright 2019, ACS.

integration (often in a sandwich structure) of stretchable electrodes with dielectrics such as a fluoropolymer gel or poly(dimethylsiloxane) (PDMS). EAPs are classified as either: i) ionic or ii) electronic, based on the driving principle. In an ionic EAP, the mechanical strain in, for example, an ionic polymer-metal composite actuator[86,87] or conducting-polymer actuator,[59,88–90] is activated by ionic drift when a voltage is applied. Under a voltage bias, the ions drift to their oppositely poled electrodes.

The difference in sizes of the ions causes one side to swell more than the other; this asymmetry leads to bending motion, as shown in Figure 2f.

Electronic EAP actuators include two types: dielectric elastomer actuators (DEAs) and piezoelectric actuators. A DEA consists of a soft insulating elastomer like PDMS sandwiched between electrodes. When a voltage is applied to the electrodes, an electrostatic force is generated, which causes the electrodes to attract, and thus a pressure to be applied to the elastomer. The conservation of volume results in an expansion of the elastomer in directions orthogonal to the electric field.[91,92] In piezoelectric actuators, a piezoelectric polymer[93,94] such as polyvinylidene fluoride is used in place of the passive PDMS. In this case, the dipoles in the piezoelectric layer actuate to extend or contract molecular chains, as shown in Figure 2g. The voltage to actuate DEAs is high (hundreds of volts), while ionic and piezoelectric EAP actuators can operate at a lower voltage (a few volts to tens of volts). A significant advantage of EAP actuators as a class is that they exhibit fast responses and corresponding frequencies in the range of kilohertz.

### 3.5. Pneumatic and Hydraulic Driven Polymeric Structures

Pneumatic and hydraulic actuators are composed of stretchable elastomers that contain compartments that can be filled with air or liquid. Under the application of pressure, the actuators exhibit deformation (extension, contraction, bending, and twisting) due to the inhomogeneous extension of layers with differential stiffness and extensibilities.[95–97] Indeed, the requirement for the realization of pneumatic and hydraulic actuators is the difference in the deformability (flexibility and stretchability) of materials and structures in the device architecture, hence there is minimal restriction on the choice of materials. Nevertheless, it remains a challenge to construct micro-scale channels inside solid polymeric structures. Moreover, pneumatic and hydraulic mechanisms require pressure to be supplied by auxiliary equipment which can be heavy and bulky.

### 3.6. Light-Driven Polymers

The most common light-driven actuator materials are based on liquid crystal polymers.[60,98,99] Similar to thermally driven LCEs, these liquid-crystal polymers are initially aligned in nematic state. When the light stimulus is applied, the liquid crystals undergo a phase transition to isotropic state, which translates into mechanical deformations. This type of material shows very high actuation stress; however, it needs to be in the form of a thin film, otherwise the light stimuli cannot penetrate through to trigger actuation. Light-stimulated actuators[60] show fast response time because of the rapid molecular transition under light stimuli. In addition, such actuators can be powered and controlled wirelessly through projected light, which is advantageous for realizing compact, untethered actuators.

**Table 1** summarizes the advantages and disadvantages of various organic actuator materials, and **Table 2** lists the typical range of mechanical properties for each actuator type. The selection of materials for haptic interfaces will depend on the required actuation stress, strain, and speed of the target application. With respect to the actuation response

**Table 1.** Categories of organic actuator materials.

| Materials | Advantages | Disadvantages | Processing methods |
|---|---|---|---|
| Hydrogels | • Ultra-high strain<br>• Can be biodegradable | • Very slow response<br>• Low stress<br>• Control resolution limited by diffusion<br>• Requires liquid environment | • Extrusion printing<br>• Molding<br>• Thin-film coating<br>• ~~Digital light processing~~ |
| Thermally driven polymers | • Stiffness can be similar to human muscles<br>• High strain with sufficient stress for haptics<br>• Simple control by tuning temperature | • Slow response<br>• Overheating issues<br>• Control resolution limited by diffusion | • Extrusion printing<br>• Molding<br>• Thin-film coating<br>• ~~Digital light processing~~ |
| Magnetic composites | • Stiffness can be similar to human muscles<br>• High strain with sufficient stress for haptics<br>• Fast response | • Requires equipment to generate magnetic field<br>• Magnetic field interference | • Extrusion printing<br>• Molding<br>• Thin-film coating |
| Electroactive polymers (electronic) | • Fast response<br>• High stress<br>• Simple control by applying voltage<br>• High control resolution | • Requires high voltage<br>• High stiffness compared to muscles<br>• Low strain for haptics | • Inkjet printing<br>• Molding<br>• Thin-film coating |
| Electroactive polymers (ionic) | • Low driving voltage High stress<br>• Simple control by applying voltage<br>• High control resolution | • Slow response<br>• High stiffness compared to muscles<br>• Low strain for haptics | • Inkjet printing<br>• Molding<br>• Thin-film coating |
| Pneumatic and hydraulic driven polymeric structures | • High stress and ultra-high strain<br>• Very fast response | • Requires tethering to equipment to apply fluidic pressure | • Inkjet printing<br>• Molding<br>• Extrusion printing |
| Light-driven polymers | • High stress<br>• Fast response<br>• Simple control by illumination | • Low strain<br>• Low output force | • Inkjet printing<br>• Thin-film coating |

**Table 2.** Typical range of mechanical characteristics for various organic actuators.

| | Maximum actuation stress [MPa] | Maximum actuation strain | Elastic modulus [MPa] | Actuation response time |
|---|---|---|---|---|
| Hydrogels | 0.04 | 50–500% | $10^{-3}$ | 5 min–10 h |
| Thermally driven polymers | 0.3–4 | 30–100% | 0.7–4 | 2 s to 1 min |
| Magnetic composites | 0.2 | 80% | 0.25–1 | ≈1 s |
| Electroactive polymers | 0.4–30 | 3–60% | 5–1400 | ≈10 ms |
| Pneumatic driven polymeric structures | 0.05–0.5 | 900% | 0.3–4 | ≈100 ms |
| ~~Light driven~~ polymers | 65 | <1% | $10^4$ | ≈100 ms |
| Human muscles | 0.1–0.6 | 15–70% | 0.1–4 | ≈60 ms |

time, the values are defined as the time to reach 90% of a full actuation stroke. Among the listed materials, hydrogels are limited by water diffusion speed and will not meet the response time needed for real-time haptic feedback. Other polymers are also limited in actuation speed due to viscoelastic characteristics universal to polymers, but they are viable for real-time haptics by using device designs that leverage snap-through instabilities,[100,101] which significantly increase the actuation speed and output forces.

For kinesthetic interfaces, materials that output high stress would be suitable for applying large force at strong joints like elbows, while materials that output low stress would be sufficient for use on finger joints to emulate gentle movement sensations. Kinesthetic interfaces in wearable devices may need to accommodate a large range of movement, and therefore it would be desirable to use materials that exhibit large strain.

On the other hand, tactile interfaces aim to tune the surface textures and morphologies, which do not necessarily require large strain, and the materials choices for tactile devices are open to a wide range of strain characteristics. The spatial resolution of tactile devices is a design consideration. Some actuation stimuli are difficult to confine spatially, for example, water diffusion in hydrogels, thermal diffusion in thermally driven polymers, and the external magnetic field to control magnetic composites. By comparison, in electroactive polymers, fluidic driven actuators, and light-driven polymers, the actuation stimuli can be applied precisely to a small area; as such, these materials are great candidates for tactile interfaces that require high spatial resolution. In addition to our suggestions here, we refer readers to the seminal paper[102] by Huber and Ashby on how to select actuators for a target application.

For organic haptic actuators interfacing with human body, different safety concerns arise depending the actuation stimuli, such as the high voltage used in electronic electroactive actuators, the high temperature to actuate thermally driven polymers, or for magnetic composites the magnetic control field that potentially interferes with nearby electronics. The detailed designs of safety features will depend on the device and application, but general efforts include keeping the voltage or heat stimuli in safe range and to isolate the stimuli from human contact. Later on, Section 5.4 will expand on safety issues.

All of the organic actuator materials discussed above can be processed by additive printing techniques. Processing methods like inkjet or thin-film coating are suitable for the formation of thin-film structures, which are desirable for electroactive or light-driven actuators to minimize the applied voltage or to ensure light penetration, respectively. Other organic actuator materials are functional as thick films and can be processed by extrusion printing. Extrusion is compatible with a wide variety of materials ranging from polymers to metallic nanoparticle composites, and it is used to pattern the various materials comprising the haptic prototypes in this report. While traditional processing methods such as molding or hot-compression are limited to simple geometries, fabrication by digital printing opens avenues to construct structures of much greater intricacy.

## 4. Digital Fabrication Methods

To fabricate haptic devices, digital printing offers the capability to additively combine structural and electronic materials so as to fabricate functional, scalable devices using a unified process. Printing can achieve free-form designs for customization of haptic interfaces, for example, to improve the fitting of a prosthesis with haptic feedback. The resolution of printed features is maintained over large areas; this capability makes it possible to scale up devices to cover the entire human body. Common printing techniques have established patterning resolution ranging from tens to hundreds of micrometers; such resolution is sufficient for tactile arrays. Extending on the estimation by Biswas and Visell,[3] if a tactile pixel array has a resolution on the order of few hundred micrometer, each pixel will trigger an individual receptor, as the maximum density of tactile receptors is ≈500 receptors/cm$^2$, roughly equivalent to 1 receptor per (400 μm).[2] The desired feature resolution and materials requirements will dictate the selection of a suitable printing method. In this section, we will survey the major categories of printing processes.

As a side note, the terminology of "4D printing" has been used recently to describe the fabrication of objects whose shape or other properties can change over time due to external stimuli.[15,103,104] The boundary between "4D printing" and "printing an actuator" is thus not distinct, and in our subsequent discussion we use the general term "printing" without reference to the dimensionality.

**Figure 3**a shows a list of common printing methods with respect to the tolerance in ink viscosity for each particular method. Ink viscosity is a key parameter that dictates whether the ink can flow out of the printer nozzle, and it can be tuned by the printing temperature and ink formulation. The formulation[105,106] of ink depends on the solute's polarity and solubility

in a solvent. The solvent can be chosen to have low boiling point to hasten evaporation, but there is a trade-off that fast evaporation may cause nozzle clogging. The various printing techniques cover inks with a range of rheological behavior, from liquid solutions to pastes to solid powders. This versatility offers options to formulate inks that can result in materials with the desired properties (e.g., electrical conductivity and mechanical response to stimuli). The quality of the printed workpiece will be affected by processing conditions such as nozzle control waveforms and temperature, the printing tool-path,[107,108] and the interfacial wettability[109] between the ink and the surface being printed on.

In addition to the methods listed in Figure 3a, screen printing[22] and gravure printing[110] are often used to pattern electronic devices, but these techniques transfer inks from a stencil mask or engraved cylinder and do not allow on-the-fly changes afforded by direct patterning from digital designs. Spray printing or aerosol jet printing[111] has been used mainly for patterning high-resolution electrical interconnects but not for polymeric structures, due to the difficulties of forming aerosol from polymers. We refer readers to the review articles in refs. [22,105,112] for a comparison of printing technologies to fabricate soft sensors and actuators.

In the following discussion, we focus on the digital printing methods that allow direct deposition of multiple functional materials, and we classify them into three broad categories—inkjet, extrusion, and photo-patterning. Inkjet and extrusion are nozzle-based methods. Inkjet is a non-contact printing process, where the nozzles do not touch the surface being printed on and is tolerant of rough surfaces. In contrast, extrusion is a contact process with the nozzles directly depositing materials over top surfaces and requires accurate control of the distance between nozzles and surfaces. Finally, photo-patterning uses light to crosslink polymers or sinter materials together. Below we present the process principles, advantages, and drawbacks of each technique.

### 4.1. Inkjet Printing

Schematic drawings of the inkjet printing process are shown in Figure 3b. These techniques comprise both the conventional approach and the electrohydrodynamic (EHD) extension. Piezo-driven inkjet printing is a mature technology and has been scaled up for mass production by using parallelized printheads with a high density of nozzles, around a few hundred nozzles per printhead. In conventional inkjet, a driving voltage waveform is applied to the piezoelectric stack in the nozzle, which triggers an acoustic or pressure wave in the ink reservoir to eject a droplet with a volume proportional to the nozzle orifice diameter, typically on the order of picoliter in volume. Because inkjet uses low-viscosity liquids (≈10 centipoise or $10^{-2}$ Pa s), the printed films tend to be thin, less than a micrometer in thickness. The ink formulations can be tuned to incorporate electronic materials; for example, semiconductors[119–121] and conductive electrodes[122–125] have been deposited by inkjet to fabricate circuits[126,127] as demonstrated in Figure 3c.[35] In addition, structural materials such as epoxy binders are commonly used in inkjet to build up 3D structures layer by layer. The resolution of the printed feature depends on the volume of ink droplets and their interaction with the substrate,[107,109] and the typical resolution is tens of micrometers.

To further improve feature resolution, inkjet printing can be modified into an EHD format, in which a pulsating electric field is used in droplet formation. A high voltage pulse is applied between the nozzle and substrate, generating a high electric field that induces a cone-shaped meniscus at the nozzle and ejects droplets considerably smaller than the nozzle orifice. Drop-on-demand EHD printing reaches resolution below 10 μm. Moreover, because of the small droplet volume with a large ratio of surface area to volume, the ink solvent evaporates quickly, limiting spread and allowing the colloidal particles to stack up vertically. The EHD method has printed metallic pillars and 3D interconnects[114] as shown in Figure 3d. However, this process tends to be slow due to the small droplet volume and the low jetting frequency of a few hundred hertz. Thus EHD printing is currently limited to research purposes or in applications that need only small, yet precise, coverage such as conductive line repairs.

### 4.2. Extrusion Printing

Extrusion processes, as shown in Figure 3e, can pattern materials from prepolymers or melts characterized by high shear viscosity (10 to $10^4$ Pa s). In this process, the precursor solidifies immediately upon exiting the nozzle. Extrusion leverages the temperature-dependent viscosity of materials. Printable materials include thermoplastic solids and composite pastes. In a technique known as fused deposition modeling, solid filaments are melted inside a heated nozzle, and the melt is extruded onto the substrate. When the thermoplastic cools below its glass transition temperature, it solidifies to form slices that constitute a 3D structure. For composite pastes, extrusion is regulated by applying pneumatic or mechanical pressure to push the material through the nozzle. The desired flow characteristics are reached by adjusting the paste viscosity, surface tension, shear moduli, and nozzle temperature. The paste is heated inside the nozzle to lower the viscosity and minimize the resistance to extrusion. Upon exiting the nozzle, the material cools and its viscosity increases, which minimizes or prevents spreading. The resolution of the features printable by extrusion is similar to the inner diameter of the nozzle, or slightly larger due to lateral spread of the printed materials, and is typically on the order of hundreds of micrometers.

Extrusion is amenable to a diverse range of materials and is the most commonly used method for printing different materials on the same platform. For conductive structures, the possible material choices include polymer composites percolated with conductive particles,[128–131] or liquid metal alloys such as eutectic indium gallium[115,132,133] that can be patterned into mesoscale structures due to a spontaneous surface oxide upon extrusion (Figure 3f). Functional devices ranging from energy storage[134,135] to optoelectronics[136,137] have been made by extrusion. For structural polymers, an advanced extrusion head, whose design is shown in Figure 3g, has enabled a flow control that switches seamlessly between multiple viscoelastic materials within a nozzle, creating voxelated elements with

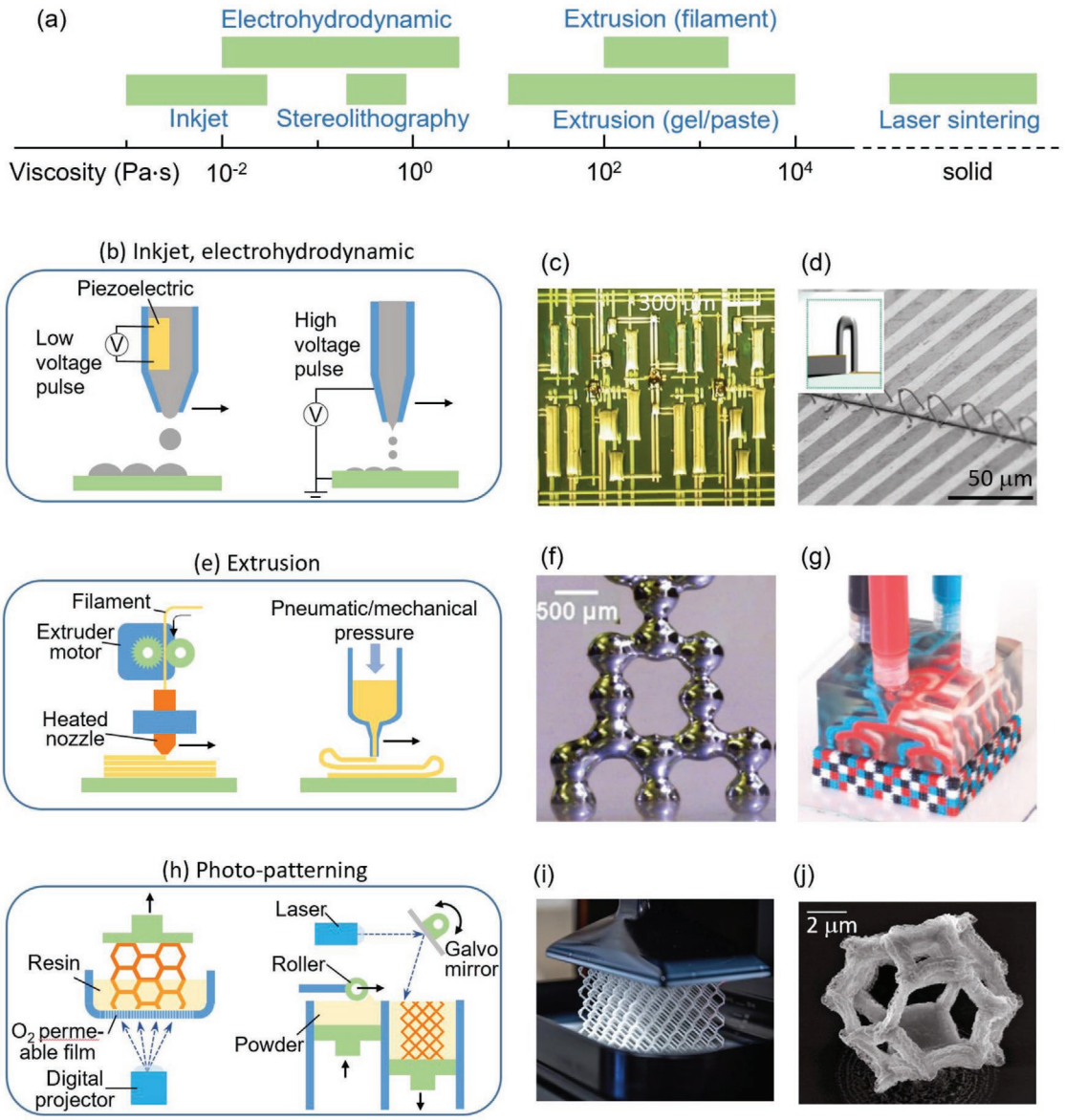


**Figure 3.** a) Digital fabrication techniques and the corresponding ink viscosities. b) Schematics of inkjet and electrohydrodynamic printing. c) Inkjet-printed circuits. d) 3D interconnects made by electrohydrodynamic inkjet. e) Schematics of extrusion printheads. The left sketch shows fused deposition modeling. The right sketch illustrates pneumatic extrusion. f) Extruded eutectic gallium indium metal structures. Reproduced with permission.[115] Copyright 2013, Wiley-VCH. g) Voxelated extrusion of multiple materials. h) Schematics of photo-patterning processes. The left sketch shows Digital Light Processing. The right sketch shows selective laser sintering. i) Photo-polymerization based on continuous liquid interface production.[117] j) Pyrolyzed nickel nanostructure patterned by two-photon lithography. c) Reproduced with permission.[113] Copyright 2013, IEEE. d) Reproduced with permission.[114] Copyright 2015, Wiley-VCH. g) Reproduced with permission.[116] Copyright 2019, Springer Nature. i) Photo reproduced with permission from Carbon3D Inc. https://www.carbon3d.com/our-technology/. j) Reproduced with permission.[118] Copyright 2019, Springer Nature.

dimensions approaching that of the cube of the nozzle diameter.[116] This multi-material nozzle can be further scaled up to multi-nozzle arrays, which greatly expand the throughput and ability to extrude structures with complex architectures.

### 4.3. Photo-Patterning

Broadly speaking, light-based patterning techniques are categorized as either light-induced polymerization or light-power sintering, as depicted in Figure 3h. Generally, each layer is patterned by illumination that locally crosslinks a volume of photocurable material.[138,139] Following crosslinking of the first layer, a new layer of liquid resin or powder is added and photo-patterned, and the process is repeated to build up the structure layer by layer. In stereolithography and selective laser sintering,[140] a digitally controlled galvo-mirror directs a laser beam to solidify the resin, or to melt powder, respectively. The powder can be metallic, ceramic, or polymeric. The schematic diagram on the right in Figure 3h shows a critical aspect of the

process, in which a thin layer of powder is pushed by a roller into the working tank. The laser then selectively sinters the desired pattern on the surface. Subsequently, the roller spreads another thin layer of powder for patterning the next layer.

In a process named continuous liquid interface production as shown in Figure 3i,[117] the UV-sensitive resin is placed in a container with an oxygen-permeable, UV-transparent window. A digital light pattern is projected onto the window. Because the resin polymerization reaction requires both UV illumination and oxygen, only a thin layer of resin next to the oxygen-permeable window may crosslink and solidify in the active zone in the presence of oxygen. The entire object is manufactured by continuously changing the pattern of projected light and pulling up the printed portion, while the surrounding liquid resin refills the active zone. This method has increased the printing speed by at least an order of magnitude and maintained high resolution around 75 μm. However, photo-patterning processes are heavily dependent on resin and currently do not allow printing multiple materials in the same layer. Nonetheless, new resin development has pushed the range of choices of materials well beyond polymers. For example, in Figure 3j, a hybrid inorganic–organic resin with nickel clusters is crosslinked by two-photon lithography to sculpt structures with sub-micrometer resolution.[118] The structure is pyrolyzed to burn off the organics, and in the process produces scaffolds which are >90 wt% Ni.

Currently, photo-patterning is ideally suited for printing mechanical structures, inkjet is likewise for printing thin-film electronics, and extrusion has been used for patterning both electronic and mechanical structures, albeit at a lower resolution than the other two techniques. In each type of printing, the patterning and solidification process define the resolution of printed features and the type of materials to which it is amenable.[105,112] To pattern multi-material structures required in haptic actuators, we developed multi-nozzle printing systems, for which it is possible to adjust printing conditions such as nozzle temperature and applied pressure, tailored to the requirements of each material. Printing processes can also be interchanged to deposit different materials. We combine extrusion printing using pastes and fused deposition modeling using filaments. These two extrusion techniques are compatible with a wide variety of organic materials and can be easily switched to deposit different materials over large areas. The next section will discuss promising approaches to address the critical issue of multi-material compatibility in the design and fabrication of haptic devices.

## 5. Challenges and Their Potential Solutions with Regard to Printing Multi-Materials Haptic Actuators

The problem of achieving the desired functionalities is dependent on the ability to heterogeneously integrate materials with different mechanical and electrical properties. For example, soft, organic actuators may require structural materials with different rigidities (to complement actuating elements with structural supports), or to harness snap-through instabilities[100,101] and increase the motion speed and output forces. As a mechatronic device, the haptic actuators with electrical controls can leverage widely accessible integrated circuits, but this aspect adds new integration challenges, such as how to form robust electrical connections and to maintain stable electrical performance under mechanical stress. The complexity of a multi-material system can make the fabrication process difficult, and new development to improve printing techniques will be essential for rapid prototyping to test new concepts. Moreover, for any human–machine interface, safety is a paramount consideration, and we will discuss designs to ensure operation within safe limits. Below we group the aforementioned challenges into four topics and present potential solutions, as listed in **Table 3**.

**Table 3.** Design and fabrication challenges in printing multi-materials actuators.

| Design and fabrication challenges | Potential solutions |
|---|---|
| Delamination or buckling due to mismatch in materials moduli | • Incorporate elasticity gradient between rigid and flexible components to relieve stress<br>• Incorporate cuts, kirigami designs, or hooked structures between interfaces<br>• Use bonding materials at interfaces, for example, a mixture of the component materials |
| Integration of electronic and mechanical functionalities | • Use composites, such as elastomers mixed with conductors to mitigate conductor cracks<br>• Place sensors, actuators, and controller chips on different substrates, then laminate or use photo-cross-linkers to bond components |
| Fidelity of printed structures in replicating digital design | • Optimize deposition by adjusting the flow rate, layer height, line-overlap ratio, and printing speed and trajectory<br>• Adjust time delay at printing start-points to ensure adequate filling; control flow at end-points to prevent materials leakage<br>• Track printed features and tune printing parameters in real-time |
| Safety of human–actuator interactions | • Operate with real-time feedback control to cut power when safety limits are exceeded<br>• Encapsulate with insulating materials to avoid electrical and thermal contacts |

### 5.1. Mismatch in Moduli

In actuators comprising multiple materials, the adhesion and mechanical moduli between material interfaces are important factors affecting structural integrity. When there is a large mismatch of mechanical moduli, the material stacks do not deform homogeneously upon actuation, resulting in interfacial stress. The stress may cause delamination or buckling of materials, or result in cracks when the stress exceeds the strength. Instead of abrupt, high-stress interfaces, the design of the structure can be adjusted to incorporate an elasticity gradient to alleviate interfacial stress, for example, by using auxetic architectures[141] or tuning the ratios of base to cross-linker in materials to gradually change the mechanical moduli at interfaces.

Alternatively, the challenge of maintaining structural integrity upon deformation can be addressed by geometric designs. For example, designs inspired by kirigami[142,143] use cuts in bendable but not stretchable films to fold and form 3D actuators. Serpentine patterns[144] are often used to enhance the stretchability of interconnects. A simple bonder could be a mixture or suspension of the materials at the interface. With more advanced material design, an adhesive that can form crosslinking bonds to both materials at an interface can be applied to joint materials.[145,146]

In addition, to bond materials without the need of adhesives, an effective solution is to design hooked structures. Similar to riveting in metalwork, the structural components have portions that intersect or interlock to hold the pieces together. We used this interlocking mechanism in the demonstration of a haptic surface shown in the figures of Section 6. Specifically, in the actuator segments, we incorporate open slots in one material such that the second material would penetrate through the slots to connect the layers above and beneath the through-hole and fasten the first material in place. The geometric designs to relieve structural issues may also be applicable for electrical components as discussed below.

### 5.2. Integration of Electronic and Mechanical Functionalities

In haptic devices, flexible conductors are needed as conductive interconnects, or to serve as resistive sensors (e.g., for sensing temperature or strain) or triggers for actuation (e.g., for joule heating or electrical bias). Silver nanoparticle paste is often used for its high flexibility, conductivity and compatibility with printing. However, conductive traces made of silver nanoparticles can crack and delaminate when stretched. To combat this issue, a simple solution is to mix a small amount (usually less than 20%) of the structural organic material into the conductive paste. The organic content in the conductive mixture will bond to the surrounding polymer structures, to prevent crack in the conductive traces and still provide high conductivity. There are significant advances in stretchable conductors, and we refer readers to the extensive reviews on this topic.[24,132,147]

In addition to interconnects, electronic integrated circuits are important for realizing haptic feedback. However, many electronic components, such as programmable silicon controllers, cannot be fabricated by direct printing and require additional integration steps.[148,149] These electronic components are usually rigid, and during actuation they can be displaced due to poor adhesion. A common method to tackle this integration challenge is to assembly the electronic components on a separate flexible substrate, and then embed the flexible electronic substrate into the neutral plane or on an unmovable part of the structure.[150] Another approach is to print a buffer elastomer to encapsulate the rigid chips and gradually release stress between rigid and soft materials to mitigate high-stress interfaces.[151]

### 5.3. Fidelity of Printing Process

The ability to digitally design and rapidly print integrated actuators is powerful for haptic research and applications. The most common technique for printing soft actuators is based on extrusion of organic materials and composites. While extrusion of pastes is versatile and compatible with many types of materials, it requires precise control of the extrusion flow rate in coordination with a well-designed tool-path (often written in G-code for computer-aided manufacturing), in order to faithfully construct the digital sketch. Optimizing the printing tool-path,[108] along with post-processing treatments, can significantly improve the workpiece fidelity to the intended design. Common approaches to achieve overhanging structures involve the use of sacrificial supporting structures that can be cut or dissolved away after fabrication, and chemical or mechanical polishing can be used to reduce surface roughness of the workpiece.

Here, we provide some suggestions to achieve better results in processes based on extrusion. Specifically for pneumatic printing, the extrusion flow rate is affected by multiple parameters including air supply pressure, nozzle dimension, and ink viscosity. To calibrate the flow rate, extrusion is run for a time period, and the weight of extruded material is measured. Then, the nozzle tool-path motion, that is, the movement velocity of the printing nozzle, should be tuned depending on the extrusion flow rate. We use the following formula to adjust the traveling velocity of the nozzle:

$$v = \frac{m}{\rho t} \cdot \frac{1}{\phi(1-\lambda)h} \tag{1}$$

where $v$ is the nozzle velocity, $m$ is the measured weight and $t$ is the time period of the extrusion calibration, $\rho$ is the density of the material being extruded, $\phi$ is the inner diameter of the nozzle, $\lambda$ is overlap ratio between neighboring traces, and $h$ is the desired height of the printed layer. This calculation is used to ensure that the right amount of material is deposited to fill the designed volume without over- or under-extrusion, as either would create defects manifested as bulges or voids, respectively, in the printed structures. If the extrusion flow rate changes over time, the nozzle velocity needs to be adjusted. In the future, it would be desirable to incorporate automated feedback control[152] that tracks the printed features and tunes the printing velocity in real-time.

Another aspect of tool-path optimization is to compensate for under-filling at the start and over-filling at the end of a printing path. Because of the high viscosity of extrusion inks, the flow of ink is delayed in time with respect to the starting time of the air pressure supply. Thus, after initiating air supply, a delay in hundreds of milliseconds should be implemented before moving the nozzle away from the starting point, to ensure enough material is deposited at the starting point. At the end point, as the air pressure is removed, there should also be a similar delay period to stabilize the flow. We also move the nozzle to areas outside of the workpiece for several millimeters at high speed (>80 mm $s^{-1}$) and high acceleration (1000 mm $s^{-2}$). The high shear rate during this sudden motion will cut off the continuity of the extruded strand, and avoid undesired residual ink being deposited on the workpiece surface.

Finally, the printing tool-path can be divided according to the desired resolution; for example, in regions where there are no complicated features, the tool path of the printhead can be in coarse resolution and speed up the printing. The tool-path design is an active area of research, and we expect more

advances in printing algorithms in the near future to improve the fidelity of printed devices to their digital designs.

### 5.4. Safety in Haptic Applications

Soft polymeric materials are great candidates for human-machine interfaces as they have similar mechanical properties as biological tissues. Nevertheless, there are safety issues to be considered in haptic applications, in case of malfunction. In actuators with electrical controls, such as DEA and LCE devices, the voltage or current supply to the actuator must be isolated from human contact. Moreover, it must have control logic to shut off power when the safety threshold is exceeded.

In particular for thermally driven actuators like SMP and LCE, it is recommended that the surface temperature of the device ≤60 °C, which is the temperature that a human can touch for up to 5 s without sustaining a burn (ASTM C1055, the Standard Guide for Heated System Surface Conditions that Produce Contact Burn Injuries). Increasing the thickness of the thermal insulation layer is an option to provide protection from thermal runaway. For actuators with an integrated heater, there can be problems arising from over-heating due to cracks in the heater. The resistance around the cracks will be much higher than in other conductive regions, and the voltage drop will be highest around the cracks, causing concentrated heat density and potentially burn the local area. To mitigate this risk, there can be real-time tracking of heater resistance to identify cracks and shut off the power supply when necessary.

For a common closed-loop system using proportional-integral-derivative (PID) controller, if an extreme event occurs like a sudden change in temperature or malfunctioning of the temperature sensor, the PID control may over-shoot or stay constantly on, leading to the possibility of overheating. To avoid accidental overheating, the safety control logic should be designed as the highest priority to cut off power to the heater, if a sensor temperature exceeds a preset safety value. If the sensor itself malfunctions, it will show up as either an open or short circuit at the sampling node; identifying such events will be critical, so that power can be terminated for safety. The above discussion is not comprehensive, but at least they are easy steps to ensure safe operation of thermally driven actuators within research settings.

## 6. Printed Organic Haptic Devices

Additive printing methods have been used to fabricate individual parts to be assembled into a haptic system, or printing is used to make the mold[37,153] for casting the actuator materials. Many of the printed haptic devices were based on pneumatic actuation, including pneumatic haptic gloves[37,40] and a tactile array[154] that combines pneumatic chambers with a SMP membrane to form a large, flexible reconfigurable surface. Below we demonstrate haptic devices using another actuation mechanism based on thermally driven polymers that enable a compact form factor. The prototypes are printed by extrusion, which allows us to directly deposit multiple materials and build entire haptic structures on automated printer platforms.

We demonstrate two examples of haptic interfaces, targeting tactile or kinesthetic senses. The main actuating material is LCE, and the actuation mechanism is based on temperature control through integrated resistive heaters. The haptic device designs incorporate non-actuating structural elements that convert the linear deformation of LCE to morph in curvilinear motion. The electronic and structural materials are patterned through a modified extrusion printer, with two pneumatic nozzles (one for LCE, another for conductive paste), two fused filament nozzles (for thermoplastic polyurethane structures), and a built-in UV light for polymer crosslinking. The fabrication method is an automated process flow customizable by digital controls; therefore the procedures can be easily repeated and scaled with affordable 3D printers.

We choose LCE as the actuator material for our haptic devices, because LCE shows similar mechanical characteristics as human muscles as seen in Figure 2a. The process of aligning the liquid crystals, namely mesogen domains, in LCE is critical to its actuation performance. In LCE slabs in the aligned state, when heat is applied as a stimulus, the slab will change into the isotropic phase and shrink along the aligned direction, generating force and mechanical work, as illustrated in Figure 2d. There are multiple methods to align liquid-crystalline materials. Common alignment techniques are plate shearing or surface rubbing,[155] which are widely adopted in liquid crystal display industries, or mechanical stretching followed by UV-activated cross-linking to fix the orientation of the mesogens.[156,157]

In extrusion printing, the shearing force at the nozzle temporarily aligns the LCE in the liquid-crystal phase.[80] Then, in this monodomain state, the LCE is cross-linked by UV light to permanently set the alignment of the mesogen. Without UV crosslinking, the monodomain alignment would gradually disappear after 1 to 2 h, with the LCE turning into polydomain by environmental thermal energy. In our research, we often purposely deposit LCE without alignment as non-actuating elements of the structure. To do this, the extruded LCE is heated to 80 °C, which disrupts the alignment of the mesogen and puts the material into isotropic phase. They turn into a polydomain state after cooling to the ambient temperature. When crosslinked in the polydomain state, the LCE will not actuate, since the randomly oriented mesogens do not move coherently. Thus, with the same LCE material, there is the option to process LCE either as an actuating component or an anchoring structural element, and the following demonstrations leverage the LCE tunability to meet both functions.

### 6.1. Compact Tactile Surface

Morphable tactile surfaces have been demonstrated for applications such as Braille display[26,34,158] and smart skins.[2,35] However, prior tactile surfaces have been limited to small coverage due to the complexities of fabrication and the need for bulky auxiliary components, particularly with fluidic actuators. Here we prototype a compact, flexible tactile surface that is scalable to large area by printing. This tactile surface is based on the concept of a seven-segment display.[159] The surface morphology is changed by varying the raised height of electronically programmable segments to form patterns for tactile perception.

*6.1.1. Structural Design and Electronic Control of the Printed LCE Tactile Surface*

**Figure 4**a is an exploded view of the printed tactile surface, and Figure 4b is a photograph of the integrated device. The material combinations and geometric layouts for each layer are depicted in Figures 4a,c. The detailed fabrication procedure is described in Supporting Information. Layer 1 is a polydomain LCE film that serves as a surface smoothing layer to encapsulate the device. In Layer 2, thermoplastic polyurethane (TPU) is deposited in the areas for the seven-segment actuator bars, while the remaining areas are filled in with polydomain LCE. Layer 3 is the only layer with the active actuation material; monodomain LCE is printed on top of the TPU areas, surrounded by polydomain LCE. The alignment of monodomain LCE is parallel to the width, that is, the short edge, of each rectangular actuating bar. When actuated, the bar width will shrink and affect deformation of the surface. In Layer 4, conductive silver composite

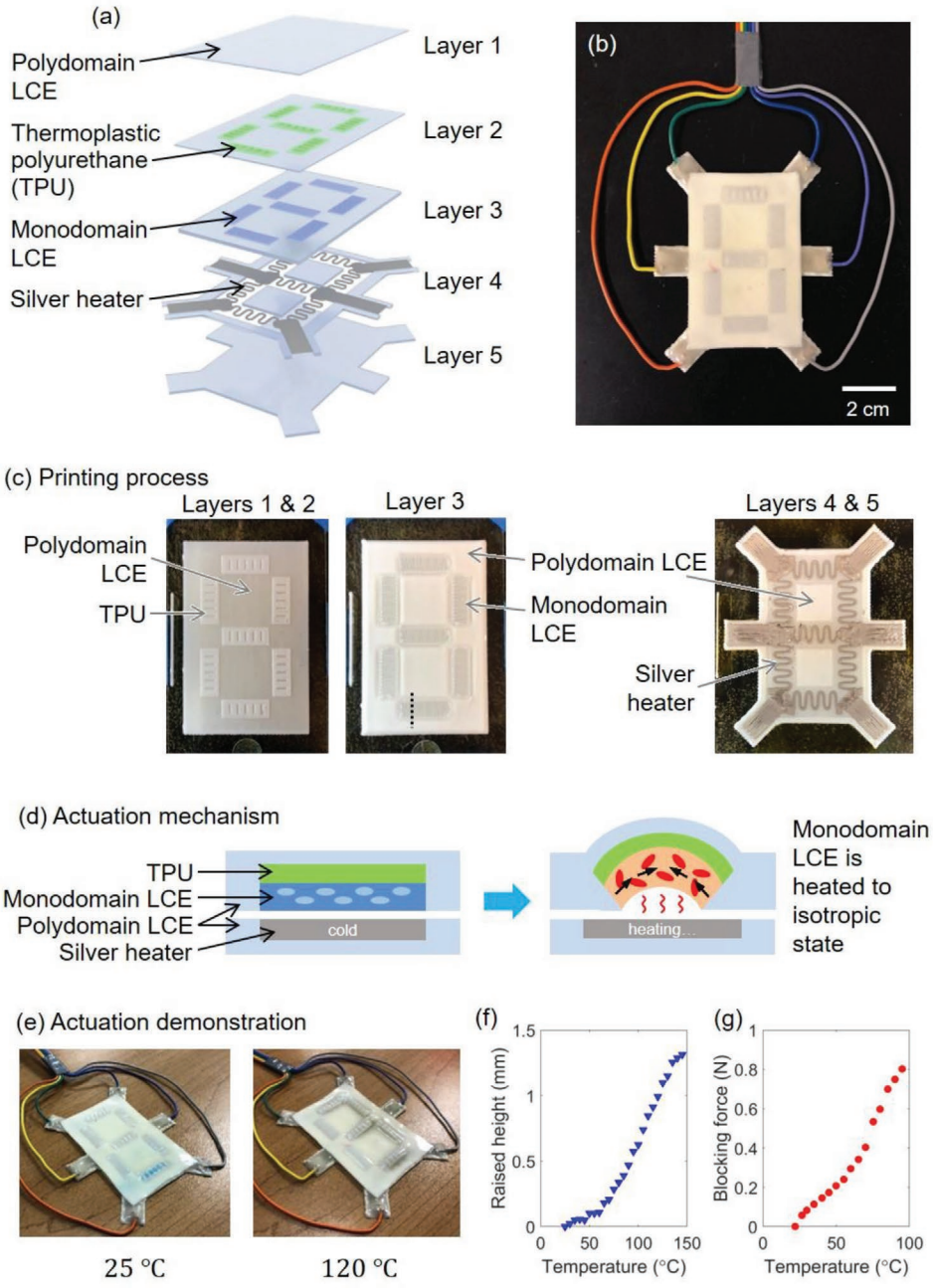


**Figure 4.** a) Exploded view and b) photograph of the printed tactile display. c) Photographs of the printed layers during the extrusion printing process. d) Cross-sectional view across an actuator segment, illustrating the actuation mechanism as temperature increases. The position of the cross-section is marked by the black dashed line in the part (c, Layer 3) photograph. e) Demonstration outputting the number "3" as corresponding segments are heated to 120 °C. f) The raised height and g) the blocking force of an actuator segment at different temperatures.

is patterned to be serpentine resistive heaters, to thermally activate the actuation of selected segments. There are six contact nodes to connect the heaters to external driver circuits. Layer 5 is another polydomain LCE film that supports the heater wires and is the bottom encapsulation for the whole device.

To power the tactile surface, electrical wires are connected to the six contact electrodes on Layer 4, and the wire inputs are controlled by discrete transistor switches. When a certain segment is selected to actuate, two wire switches are turned on, to supply dc power to the corresponding heater. The heater resistance is about 2 Ω, and the voltage is adjusted to achieve 3 W power on each heater, which can heat an actuator to more than 150 °C. When multiple segments are required to actuate together, the transistors switch on in sequence to ensure the same heating duty cycle for all the selected heaters.

#### *6.1.2. Tactile Surface Operation*

Figure 4d illustrates the actuation mechanism of tactile surface, shown as a cross-sectional view across the width of an actuator segment. The heater at the bottom does not move, whereas the actuator on top is free. The actuator layer is bonded to the bottom heater layer, but only in areas (not depicted in the cross-sectional diagram) away from the seven-segment actuators to leave space to accommodate the changes in shape. Inside each actuator bar, the layers of TPU and monodomain LCE are tightly bonded together. The upper TPU layer is a bendable but incompressible structure. When the monodomain LCE is heated, it shrinks in the horizontal direction with contraction stress. However, because the top TPU material is incompressible, there is a vertical stress gradient, with the top of the actuator bar restrained to its original length while the LCE contracting at the bottom. Therefore, the TPU-LCE actuator bar deforms to an arch shape, raised up in the middle and bent downward at the sides. This design is similar to another work using DEA[160] that leveraged stress gradient to form bumps, and here the operational voltage is 3 V, which is much lower than DEAs. The TPU-LCE combination converts LCE's linear contraction to surface morphological changes, and the seven-segment interface is electronically programmable to output different numbers as relief patterns in Video S1, Supporting Information.

Figure 4e shows an example of the tactile surface actuated to raise a number "3" pattern. When the heaters are powered on, in about 1 minute, the segments are heated from room temperature to 120 °C, as measured by an infrared camera monitoring the top surface. The change in peak height at the actuator segment with respect to surrounding non-actuated regions is measured against the surface temperature in Figure 4f. A maximum height of 1.3 mm is observed at 150 °C. Figure 4g exhibits the blocking force of one unit constrained at 0 mm height. A maximum blocking force of 0.83 N is reached at 100 °C. However, obviously for safety, we would not operate at such high temperature. It was shown that people can differentiate surface heights on the order of micrometers.[3] The surface temperature should be limited to below 60 °C, which would raise the tactile surface by a few hundred micrometers, enough morphological changes for a user to sense, based on the perception thresholds of users. Moreover, to operate well within the temperature range for skin contact, the tactile surface can be adjusted by using LCE that actuates at lower temperature and/or adding thicker heat isolation layer in the future.

In our tactile surface which is relatively large in area, thermal interference between different units is not observed. However, the spatial resolution in an array may eventually be limited by the heat gradient distribution. Heat from an actuated unit can spread to neighboring units and may interfere with their operation. The manipulation and concentration of heat flux using metamaterial cells[161,162] may be needed in order to direct thermal conduction and in turn improve the resolution of tactile arrays.

### 6.2. Lightweight Kinesthetic Glove

Kinesthetic gloves driven by fluidic pressure actuators[36–38] have shown high output force and fast response, but the bulky exoskeletons reduce user movement and comfort. Recent works aim to improve the form factor of kinesthetic gloves, to make them compact by using slim electrostatic brakes[29] or materials with tunable stiffness.[39] These devices apply damping resistance to finger joints and operate only reactively. That is, a person must initiate movement to feel the dampening effect, as the device cannot actively move the finger joint but only adjust the countering resistance. To enable a kinesthetic glove that actively applies force on the user's body, here we demonstrate a lightweight actuator based on LCE, to take advantage of the flexibility and compactness of printed LCE integrated structures.

#### *6.2.1. Structural Design of the LCE Actuator for Kinesthetic Feedback*

**Figure 5**a shows the kinesthetic actuator consisting of three printed layers. The top and bottom layers are extruded as monodomain LCE. For the middle layer, conductive silver composite is extruded to pattern the heater traces, and the areas around the heater are filled by LCE. Two pieces of copper wires are embedded in the middle layer to connect the heater loop to an external power supply. In Figure 5a, the LCE in the light blue regions is aligned parallel to the long edge of the actuator, whereas in the dark blue regions, the LCE is aligned parallel to the short edge. The perpendicular alignment directions between the dark and light blue regions reduce the axial movement of the copper wires with respect to the heater traces, to avoid disconnection in the electrical path upon actuation. A DC power supply is used to power on the integrated heater to raise the actuator temperature and control actuation.

#### *6.2.2. Characterization of the Printed LCE Actuator*

The actuator characteristics is determined in terms of temperature, stress, and strain, as shown in Figure 5b. Figure 5c show photographs of the integrated LCE actuator contracted to different lengths at various temperatures. The characterization procedure is described in the Supporting Information. The actuator

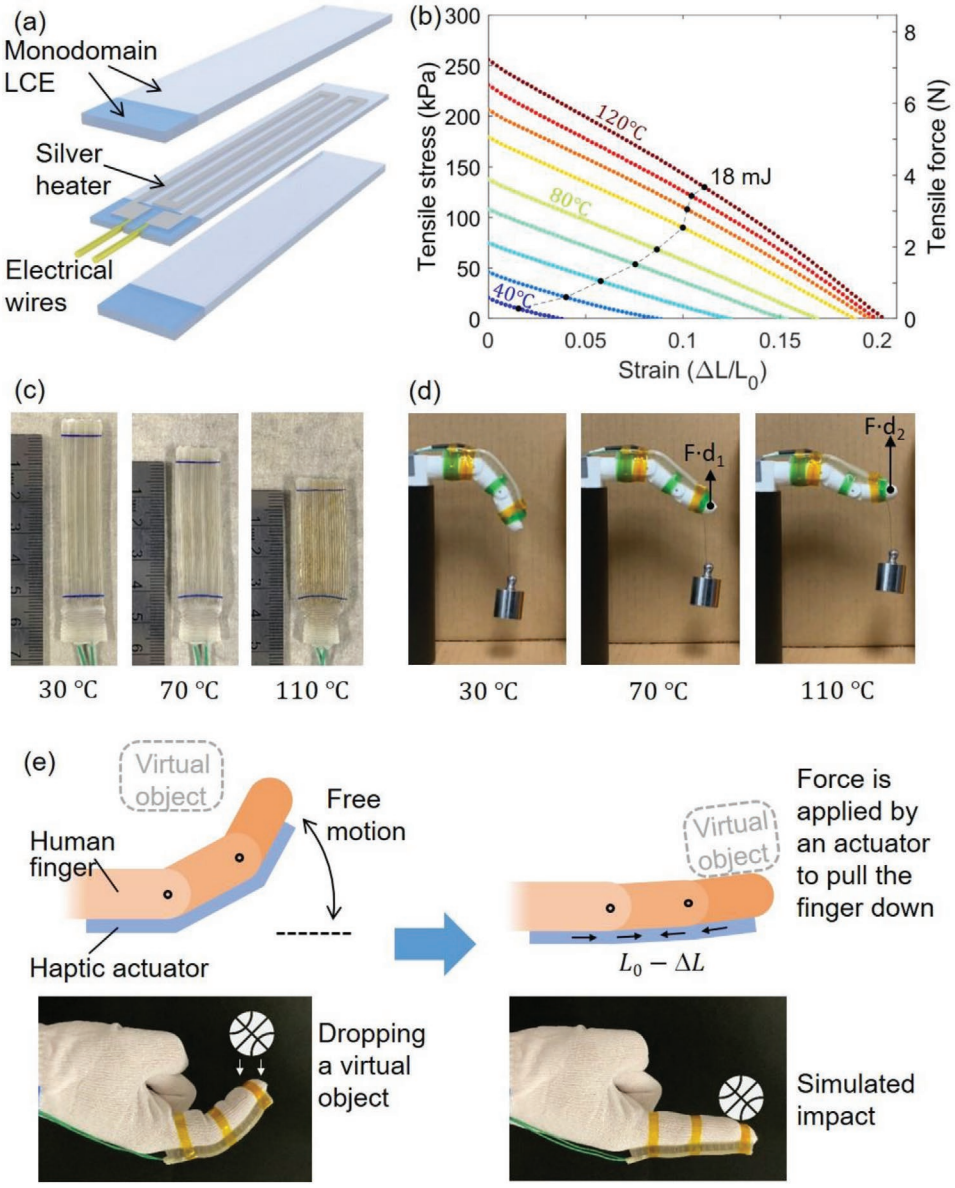


**Figure 5.** a) Exploded view of the printed kinesthetic actuator. b) Output stress–strain characteristics of the printed kinesthetic actuator at different temperatures, in steps of 10 °C. The maximum work output is marked as a black point on each curve. c) Photographs of the kinesthetic actuator when heated to different temperatures with no load. The ruler's numbers are in centimeter unit. The actuator dimensions are 70 mm in length, 12 mm in width, and 2.2 mm in thickness. d) Demonstration of actuation on a finger model. A 50 g weight is lifted by the actuator to different distances, depending on the control temperatures. e) Tensile force on the finger is applied by the actuator to generate a kinesthetic sensation, to mimic the impact from an object in virtual reality.

strain is defined as $(L_0 - \mathrm{L})/L_0$, where $L_0$ is the original length at room temperature and $L$ is the length at a certain temperature and applied stress, and $\Delta L = L_0 - \mathrm{L}$. In Figure 5b, the stress-strain measurements at a constant temperature are indicated in one color. Raising the device temperature increases the output stress and strain. The y-intercept is the blocking stress, which is the maximum force per unit area that the actuator is able to generate. At 120 °C, the actuator in Figure 5b shows a blocking stress of 255 kPa (equivalent to 7 N force). The actuator dimensions are 70 mm in length, 12 mm in width, and 2.2 mm in thickness. The stored stress is released and reduced when the actuator is allowed to contract in length, reaching the maximum strain at the $x$-intercept where no load is applied to the actuator. This actuator at 120 °C is capable of outputting 18 mJ of work (force $F$ multiplied by displacement $d$), which corresponds to lifting up against gravity a load of 370 g by a distance of 5 mm.

To demonstrate the work that the LCE actuator can do, we attach the actuator onto a model finger as shown in Figure 5d. A 50 g weight is hung on the fingertip. As the actuator is heated, the LCE contracts and lifts up the finger tip. A video of this demonstration is included as Video S2, Supporting Information. At 70 °C, the actuator lifts the finger with the 50 g weight

by 9.2 mm, corresponding to a work output of 4.5 mJ. This level of work output is generally sufficient for haptic interfaces.

The response time of thermally driven LCE actuator is limited by the heat flux exchange speed. The energy required to heat the actuator from room temperature to the actuation temperature can be estimated by $Q = c \times m \times \Delta T$, where $c$ is the specific heat capacity of the LCE (≈1 J $g^{-1}$ $K^{-1}$), $m$ is the mass of the LCE actuator (2 g), and $\Delta T$ is the temperature difference between the unheated and heated states. Therefore, the required thermal energy is estimated to be 150 J for heating the actuator from 25 to 100 °C. When the power passing through the printed silver heater is limited to <5 W as done in the above example, the heating and actuation process takes at least 30 s. This calculation assumes no heat loss and homogeneous heating. A potential method to accelerate the LCE response time is to use a high-power heater; for instance, with a 50 W heater, the temperature can be raised in 3 s if heat dissipation into the environment is minimized. In such design, the heater controller must be responsive to precisely control the temperature and input energy to avoid overheating. Conversely, the cooling process also restricts the actuator response speed. As natural cooling is slow, convection or thermoelectric cooler might be used to accelerate cooling. Overall, device geometries that maximize heat transfer would be beneficial to improve the actuator speed.

#### *6.2.3. Mechanism to Emulate Kinesthetic Sensation on a Finger*

To use the LCE actuator to offer kinesthetic feedback, we attach the actuator to the dorsal side of a fabric glove, with a 3 mm thick PDMS buffer pad to provide thermal insulation between the LCE actuator and the glove and ensure that the fabric temperature is always below 60 °C. With the LCE at room temperature, the actuator is at original length. A person wearing the kinesthetic glove can move one's finger freely, as shown in the left column of Figure 5e. In virtual reality, this scenario corresponds to the feeling that the finger is not in contact with any virtual object, and so the finger joints would feel no resistance to movement. To change the kinesthetic perception, the LCE actuator is heated to shrink its length, which pulls the finger to straighten up and restricts its free movement, as depicted in the right column of Figure 5e. This output force creates a sensation in the finger that it is pressed down by a virtual object. This actuation mechanism is able to simulate the impact of a virtual object on the user, because the LCE actuator can actively apply force in addition to passive damping of joint motion. For example, when a virtual ball is dropped onto the finger, the physical dynamics can be imitated by a rapid force pulling back the finger. We envision that the active force from the LCE glove can recreate the sensation of holding an object that moves, such as the feel of a wiggling virtual pet for entertainment or the impression of softness and resistance of the various tissues in virtual surgical training.

## 7. Conclusions

To advance a new generation of soft haptic interfaces, one promising approach as presented herein is to combine the advantages of organic actuator materials and additive printing technologies. This powerful combination can lead to devices that are ergonomic, readily customizable, and economical for everyone to explore potential benefits and create new haptic applications. Here we discuss our progress in achieving compact, lightweight haptic actuators by using an open-source extrusion printer to integrate different polymers and composites in freeform designs. We demonstrated two examples, a tactile surface and a kinesthetic glove, to show that printing with organic materials is a versatile approach to rapidly prototype various types of programmable haptic interfaces.

In the development of organic haptic actuators, we encountered fabrication challenges in the printing process and in materials compatibility. In particular, improvements in printing tool-path control, such as optimizing the extrusion height and the travel speed of nozzles to compensate for over- or under-extrusion, were implemented to raise the fidelity of printed structures to their digital blueprints. With regard to the issue of materials compatibility, delamination and cracking at materials interfaces were key problems. We compensated for poor adhesion by using mechanical hooking designs. And, specifically for electronic materials, we mixed the conductive silver ink with a small amount of the structural material. The conductive ink would bond with the surrounding structural material, and thus the conductive traces remained robustly bonded during actuation. Potentially our solutions to the above printing challenges would be relevant for other similar works on additive manufacturing of multi-material structures.

In applying organic materials to haptic applications, we note there are properties that need further improvement. Specifically for thermally actuated materials such as LCE and SMP, the key bottlenecks are the response speed and the operational temperature. Regarding the response speed, the actuation transition currently takes several to tens of seconds to complete, because the heat flow is slow and restricted by the efficiency of the integrated heater/cooler in the actuator. More effective heat transfer structures are needed for these thermally driven materials to reach better response speed, targeting millisecond transitions to be comparable to motor-driven haptic devices. The combination of rigid supports with soft actuators can also be designed to harness snap-through instabilities[100,101] in order to increase the motion speed.

Regarding the operational temperature, currently most LCE materials require temperatures much higher than 60 °C to shift from liquid-crystal to isotropic phase. Usually a thick thermal insulation layer is used so that the surface temperature is lowered to a safe level for skin contact. However, a better approach will be to adjust the formulations of LCE so that the phase transition temperature can be lowered.[163] A recent study has successfully reduced the LCE phase transition temperature by more than 30 °C through tuning the mesogen and spacer moieties.[76] With a low transition temperature, the heat required for LCE actuation is greatly reduced, ensuring thermal safety. In addition, as the phase transition requires less energy transfer, the LCE actuators will show faster response speed and consume less power. With the blooming communities of ingenious researchers working on high-performance organic actuators and printing technologies, we believe that the aforementioned issues are solvable, and the use of organic haptic interfaces,

maybe extending to a whole body suit, will be technologically possible to offer immersive haptic experiences in the future.

## Supporting Information

Supporting Information is available from the Wiley Online Library or from the author.

## Acknowledgements

Some of the original research discussed in this report was supported by Center for Wearable Sensors (CWS) at UC San Diego. The authors acknowledge support from the current member companies of CWS: Cubic, Dexcom, Gore, Honda, Huami, Kureha, Merck KGaA, Pepsico, Samsung, and Sony.

## Conflict of Interest

The authors declare no conflict of interest.

## Keywords

haptics, kinesthetic actuators, printing, soft actuators, tactile surfaces

Received: April 14, 2020
Revised: July 7, 2020
Published online:

[1] H. Culbertson, S. B. Schorr, A. M. Okamura, *Annu. Rev. Control, Rob., Auton. Syst.* **2018**, *1*, 385.
[2] X. Yu, Z. Xie, Y. Yu, J. Lee, A. Vazquez-Guardado, H. Luan, J. Ruban, X. Ning, A. Akhtar, D. Li, B. Ji, Y. Liu, R. Sun, J. Cao, Q. Huo, Y. Zhong, C. Lee, S. Kim, P. Gutruf, C. Zhang, Y. Xue, Q. Guo, A. Chempakasseril, P. Tian, W. Lu, J. Jeong, Y. Yu, J. Cornman, C. Tan, B.-H. Kim, K.-H. Lee, X. Feng, Y. Huang, J. A. Rogers, *Nature* **2019**, *575*, 473.
[3] S. Biswas, Y. Visell, *Adv. Mater. Technol.* **2019**, *4*, 1900042.
[4] D. J. Lipomi, C. Dhong, C. W. Carpenter, N. B. Root, V. S. Ramachandran, *Adv. Funct. Mater.* **2019**, *30*, 1906850.
[5] C. Pacchierotti, S. Sinclair, M. Solazzi, A. Frisoli, V. Hayward, D. Prattichizzo, *IEEE Tran. Haptics* **2017**, *10*, 580.
[6] H. P. Saal, S. J. Bensmaia, *Trends Neurosci.* **2014**, *37*, 689.
[7] R. S. Johansson, J. R. Flanagan, *Nat. Rev. Neurosci.* **2009**, *10*, 345.
[8] J. C. Tuthill, E. Azim, *Curr. Biol.* **2018**, *28*, R194.
[9] I. Matei, S. Nelaturi, E. M. Chow, J. P. Lu, J. A. Bert, L. S. Crawford, *J. Microelectromech. Syst.* **2019**, *28*, 643.
[10] J. A. Paulson, A. Mesbah, X. Zhu, M. C. Molaro, R. D. Braatz, *J. Process Control* **2015**, *27*, 38.
[11] F. Claeyssen, R. L.e Letty, F. Barillot, O. Sosnicki, *Ferroelectrics* **2007**, *351*, 3.
[12] T. R. Shrout, S. J. Zhang, *J. Electroceram.* **2007**, *19*, 185.
[13] W. J. Choi, Y. Jeon, J. H. Jeong, R. Sood, S. G. Kim, *J. Electroceram.* **2006**, *17*, 543.
[14] R. L. Truby, J. A. Lewis, *Nature* **2016**, *540*, 371.
[15] X. Kuang, D. J. Roach, J. Wu, C. M. Hamel, Z. Ding, T. Wang, M. L. Dunn, H. J. Qi, *Adv. Funct. Mater.* **2019**, *29*, 1805290.
[16] R. Su, S. H. Park, Z. Li, M. C. McAlpine, in *Robotic Systems and Autonomous Platforms*, Elsevier, New York **2019**, pp. 309–334.
[17] S. Li, H. Bai, R. F. Shepherd, H. Zhao, *Angew. Chem.* **2019**, *58*, 11182.
[18] P. A. G. S. Giachini, S. S. Gupta, W. Wang, D. Wood, M. Yunusa, E. Baharlou, M. Sitti, A. Menges, *Sci. Adv.* **2020**, *6*, eaay0929.
[19] D. Raviv, W. Zhao, C. McKnelly, A. Papadopoulou, A. Kadambi, B. Shi, S. Hirsch, D. Dikovsky, M. Zyracki, C. Olguin, R. Raskar, S. Tibbits, *Sci. Rep.* **2015**, *4*, 7422.
[20] A. D. Valentine, T. A. Busbee, J. W. Boley, J. R. Raney, A. Chortos, A. Kotikian, J. D. Berrigan, M. F. Durstock, J. A. Lewis, *Adv. Mater.* **2017**, *29*, 1703817.
[21] Y. Dong, C. Bao, W. S. Kim, *Joule* **2018**, *2*, 579.
[22] Y. Khan, A. Thielens, S. Muin, J. Ting, C. Baumbauer, A. C. Arias, *Adv. Mater.* **2019**, 1905279.
[23] B. C. K. Tee, J. Ouyang, *Adv. Mater.* **2018**, *30*, 1802560.
[24] J. Wang, M. F. Lin, S. Park, P. S. Lee, *Mater. Today* **2018**, *21*, 508.
[25] O. Bau, I. Poupyrev, A. Israr, C. Harrison, in *UIST 2010 – 23rd ACM Symp. on User Interface Software and Technology*, ACM, New York **2010**, pp. 283–292.
[26] Y. Kato, T. Sekitani, M. Takamiya, M. Doi, K. Asaka, T. Sakurai, T. Someya, *IEEE Trans. Electron Devices* **2007**, *54*, 202.
[27] R. M. Pierce, E. A. Fedalei, K. J. Kuchenbecker, in *IEEE Haptics Symp., HAPTICS*, IEEE, Piscataway, NJ, USA **2014**, pp. 19–25.
[28] S. B. Schorr, A. M. Okamura, in *Conf. on Human Factors in Computing Systems – Proc.*, ACM, New York **2017**, pp. 3115–3119.
[29] R. Hinchet, V. Vechev, H. Shea, O. Hilliges, E. Zurich, in *The 31st Annual ACM Symp. on User Interface Software and Technology*, ACM, New York **2018**, pp. 901–912.
[30] M. Ayyildiz, M. Scaraggi, O. Sirin, C. Basdogan, B. N. J. Persson, *Proc. Natl. Acad. Sci. USA* **2018**, *115*, 12668.
[31] T. Han, F. Anderson, P. Irani, T. Grossman, in *UIST 2018 – Proc. of the 31st Annual ACM Symp. on User Interface Software and Technology*, ACM, New York **2018**, pp. 913–925.
[32] O. Caldiran, H. Z. Tan, C. Basdogan, *IEEE Haptics Symp., HAPTICS*, IEEE, Piscataway, NJ, USA **2018**, p. 222.
[33] K. Fukuda, T. Sekitani, U. Zschieschang, H. Klauk, K. Kuribara, T. Yokota, T. Sugino, K. Asaka, M. Ikeda, H. Kuwabara, T. Yamamoto, K. Takimiya, T. Fukushima, T. Aida, M. Takamiya, T. Sakurai, T. Someya, *Adv. Funct. Mater.* **2011**, *21*, 4019.
[34] Y. Qiu, Z. Lu, Q. Pei, *ACS Appl. Mater. Interfaces* **2018**, *10*, 24807.
[35] J. H. Pikul, S. Li, H. Bai, R. T. Hanlon, I. Cohen, R. F. Shepherd, *Science* **2017**, *358*, 210.
[36] Z. Ma, P. Ben-Tzvi, *J. Mech. Rob.* **2015**, *7*, 041008.
[37] S. Jadhav, B. Kang, V. Kannanda, M. T. Tolley, J. P. Schulze, *Electron. Imaging* **2017**, *2017*, 19.
[38] J. Iqbal, N. G. Tsagarakis, D. G. Caldwell, *Electron. Lett.* **2015**, *51*, 888.
[39] C. W. Carpenter, S. T. M. Tan, C. Keef, K. Skelil, M. Malinao, D. Rodriquez, M. A. Alkhadra, J. Ramírez, D. J. Lipomi, *Sens. Actuators, A* **2019**, *288*, 79.
[40] B. W. K. Ang, C. H. Yeow, in *IEEE Int. Conf. on Intelligent Robots and Systems*, IEEE, Piscataway, NJ, USA **2017**, pp. 1219–1223.
[41] L. Cappello, J. T. Meyer, K. C. Galloway, J. D. Peisner, R. Granberry, D. A. Wagner, S. Engelhardt, S. Paganoni, C. J. Walsh, *J. NeuroEng. Rehabil.* **2018**, *15*, 59.
[42] K. Rangarajan, H. Davis, P. Pucher, *J. Surg. Educ.* **2020**, *77*, 337.
[43] J. Shintake, V. Cacucciolo, D. Floreano, H. S. R. G. Shea, *Adv. Mater.* **2018**, *30*, 1707035.
[44] M. C. E. Alarcón, F. Ferrise, in *Proc. of the 2017 Int. Conf. on Innovative Design and Manufacturing*, Politecnico di Milano, Milan **2017**, pp. 1–6.
[45] G. Z. Yang, J. Bellingham, P. E. Dupont, P. Fischer, L. Floridi, R. Full, N. Jacobstein, V. Kumar, M. McNutt, R. Merrifield, B. J. Nelson, B. Scassellati, M. Taddeo, R. Taylor, M. Veloso, Z. L. Wang, R. Wood, *Sci. Rob.* **2018**, *3*, eaar7650.
[46] M. Cianchetti, C. Laschi, A. Menciassi, P. Dario, *Nat. Rev. Mater.* **2018**, *3*, 143.
[47] T. J. Wallin, J. Pikul, R. F. Shepherd, *Nat. Rev. Mater.* **2018**, *3*, 84.
[48] H. Wang, M. Totaro, L. Beccai, *Adv. Sci.* **2018**, *5*, 1800541.

[49] S. Wang, J. Y. Oh, J. Xu, H. Tran, Z. Bao, *Acc. Chem. Res.* **2018**, *51*, 1033.
[50] B. C.-K. Tee, A. Chortos, A. Berndt, A. K. Nguyen, A. Tom, A. McGuire, Z. C. Lin, K. Tien, W.-G. Bae, H. Wang, P. Mei, H.-H. Chou, B. Cui, K. Deisseroth, T. N. Ng, Z. Bao, *Science* **2015**, *350*, 313.
[51] Y. Cao, Y. J. Tan, S. Li, W. W. Lee, H. Guo, Y. Cai, C. Wang, B. C.-K. Tee, *Nat. Electron.* **2019**, *2*, 75.
[52] M. Amit, R. K. Mishra, Q. Hoang, A. M. Galan, J. Wang, T. N. Ng, *Mater. Horiz.* **2019**, *6*, 604.
[53] M. Amit, L. Chukoskie, A. J. Skalsky, H. Garudadri, T. N. Ng, *Adv. Funct. Mater.* **2019**, 1905241.
[54] K. M. Wiggins, J. N. Brantley, C. W. Bielawski, *Chem. Soc. Rev.* **2013**, *42*, 7130.
[55] R. Moser, G. Kettlgruber, C. M. Siket, M. Drack, I. M. Graz, U. Cakmak, Z. Major, M. Kaltenbrunner, S. Bauer, *Adv. Sci.* **2016**, *3*, 1500396.
[56] G. J. Gerling, S. C. Hauser, B. R. Soltis, A. K. Bowen, K. D. Fanta, Y. Wang, *IEEE Trans. Haptics* **2018**, *11*, 498.
[57] Comparison of EAPs with Other Actuator Technologies, http://ndeaa.jpl.nasa.gov/nasa-nde/lommas/eap/actuators-comp.pdf (accessed: ~~February 2011~~).
[58] L. Wang, Y. Yang, Y. Chen, C. Majidi, F. Iida, E. Askounis, Q. Pei, *Mater. Today* **2018**, *21*, 563.
[59] F. Hu, Y. Xue, J. Xu, B. Lu, *Front. Rob. AI* **2019**, *6*, 114.
[60] M. Camacho-Lopez, H. Finkelmann, P. Palffy-Muhoray, M. Shelley, *Nat. Mater.* **2004**, *3*, 307.
[61] F. N. Muya, C. E. Sunday, P. Baker, E. Iwuoha, *Water Sci. Technol.* **2016**, *73*, 983.
[62] A. Lendlein, S. Kelch, *Angew. Chem., Int. Ed.* **2002**, *41*, 2034.
[63] C. Yuan, D. J. Roach, C. K. Dunn, Q. Mu, X. Kuang, C. M. Yakacki, T. J. Wang, K. Yu, H. J. Qi, *Soft Matter* **2017**, *13*, 5558.
[64] Y. Kim, H. Yuk, R. Zhao, S. A. Chester, X. Zhao, *Nature* **2018**, *558*, 274.
[65] Y. Qiu, E. Zhang, R. Plamthottam, Q. Pei, *Acc. Chem. Res.* **2019**, *52*, 316.
[66] Z. Jiang, B. Diggle, I. C. G. Shackleford, L. A. Connal, *Adv. Mater.* **2019**, *31*, 1904956.
[67] J. Shang, X. Le, J. Zhang, T. Chen, P. Theato, *Polym. Chem.* **2019**, *10*, 1036.
[68] A. S. Gladman, E. A. Matsumoto, R. G. Nuzzo, L. Mahadevan, J. A. Lewis, *Nat. Mater.* **2016**, *15*, 413.
[69] C. Wang, K. Sim, J. Chen, H. Kim, Z. Rao, Y. Li, W. Chen, J. Song, R. Verduzco, C. Yu, *Adv. Mater.* **2018**, *30*, 1706695.
[70] M. Zarek, M. Layani, I. Cooperstein, E. Sachyani, D. Cohn, S. Magdassi, *Adv. Mater.* **2016**, *28*, 4449.
[71] X. Wang, X. Guo, J. Ye, N. Zheng, P. Kohli, D. Choi, Y. Zhang, Z. Xie, Q. Zhang, H. Luan, K. Nan, B. H. Kim, Y. Xu, X. Shan, W. Bai, R. Sun, Z. Wang, H. Jang, F. Zhang, Y. Ma, Z. Xu, X. Feng, T. Xie, Y. Huang, Y. Zhang, J. A. Rogers, *Adv. Mater.* **2019**, *31*, 1805615.
[72] C. S. Haines, M. D. Lima, N. Li, G. M. Spinks, J. Foroughi, J. D. W. Madden, S. H. Kim, S. Fang, M. J. De Andrade, F. Göktepe, Ö. Göktepe, S. M. Mirvakili, S. Naficy, X. Lepró, J. Oh, M. E. Kozlov, S. J. Kim, X. Xu, B. J. Swedlove, G. G. Wallace, R. H. Baughman, *Science* **2014**, *343*, 868.
[73] J. W. L. Zhou, H. Y. Chan, T. K. H. To, K. W. C. Lai, W. J. Li, *IEEE/ASME Trans. Mechatronics* **2004**, *9*, 334.
[74] T. Ebefors, E. Kälvesten, G. Stemme, *Sens. Actuators, A* **1998**, *67*, 199.
[75] T. H. Ware, M. E. McConney, J. J. Wie, V. P. Tondiglia, T. J. White, *Science* **2015**, *347*, 982.
[76] M. O. Saed, C. P. Ambulo, H. Kim, R. De, V. Raval, K. Searles, D. A. Siddiqui, J. M. O. Cue, M. C. Stefan, M. R. Shankar, T. H. Ware, *Adv. Funct. Mater.* **2019**, *29*, 1806412.
[77] A. Kotikian, R. L. Truby, J. W. Boley, T. J. White, J. A. Lewis, *Adv. Mater.* **2018**, *30*, 1706164.
[78] C. P. Ambulo, J. J. Burroughs, J. M. Boothby, H. Kim, M. R. Shankar, T. H. Ware, *ACS Appl. Mater. Interfaces* **2017**, *9*, 37332.
[79] Y. Wang, Z. Wang, Q. He, P. Iyer, S. Cai, *Adv. Intell. Syst.* **2020**, *2*, 1900177.
[80] E. C. Davidson, A. Kotikian, S. Li, J. Aizenberg, J. A. Lewis, *Adv. Mater.* **2020**, *32*, 1905682.
[81] C. Zhang, X. Lu, G. Fei, Z. Wang, H. Xia, Y. Zhao, *ACS Appl. Mater. Interfaces* **2019**, *11*, 44774.
[82] W. Hu, G. Z. Lum, M. Mastrangeli, M. Sitti, *Nature* **2018**, *554*, 81.
[83] S. Sundaram, M. Skouras, D. S. Kim, L. van den Heuvel, W. Matusik, *Sci. Adv.* **2019**, *5*, eaaw1160.
[84] J. Thévenot, H. Oliveira, O. Sandre, S. Lecommandoux, *Chem. Soc. Rev.* **2013**, *42*, 7099.
[85] Q. Ze, X. Kuang, S. Wu, J. Wong, S. M. Montgomery, R. Zhang, J. M. Kovitz, F. Yang, H. J. Qi, R. Zhao, *Adv. Mater.* **2020**, *32*, 1906657.
[86] J. D. Carricoa, N. W. Traeden, M. Aureli, K. K. Leang, *Smart Mater. Struct.* **2015**, *24*, 125021.
[87] K. Kwon, T. N. Ng, *Org. Electron.* **2014**, *15*, 294.
[88] D. Melling, J. G. Martinez, E. W. H. Jager, *Adv. Mater.* **2019**, *31*, 1808210.
[89] E. W. H. Jager, E. Smela, O. Inganas, *Science* **2000**, *290*, 1540.
[90] T. F. Otero, J. G. Martinez, J. Arias-Pardilla, *Electrochim. Acta* **2012**, *84*, 112.
[91] A. Chortos, E. Hajiesmaili, J. Morales, D. R. Clarke, J. A. Lewis, *Adv. Funct. Mater.* **2020**, *30*, 1907375.
[92] *Electroactive Polymer Actuators as Artificial Muscles: Reality, Potential, and Challenges* (Ed: Y. Bar-Cohen), SPIE Press, Washington, DC, USA **2004**.
[93] R. E. Cohen, *Nature* **2018**, *562*, 48.
[94] B. Bera, M. D. Sarkar, *IOSR J. Appl. Phys.* **2017**, *09*, 95.
[95] M. Schaffner, J. A. Faber, L. Pianegonda, P. A. Rühs, F. Coulter, A. R. Studart, *Nat. Commun.* **2018**, *9*, 878.
[96] A. Miriyev, K. Stack, H. Lipson, *Nat. Commun.* **2017**, *8*, 596.
[97] D. K. Patel, A. H. Sakhaei, M. Layani, B. Zhang, Q. Ge, S. Magdassi, *Adv. Mater.* **2017**, *29*, 1606000.
[98] K. W. Kwan, S. J. Li, N. Y. Hau, W. D.i Li, S. P. Feng, A. H. W. Ngan, A. H. Gelebart, D. J. Mulder, G. Vantomme, A. P. H. J. Schenning, D. J. Broer, *Angew. Chem., Int. Ed.* **2017**, *3*, 13436.
[99] Z. Cheng, T. Wang, X. Li, Y. Zhang, H. Yu, *ACS Appl. Mater. Interfaces* **2015**, *7*, 27494.
[100] J. T. B. Overveldea, T. Kloeka, J. J. A. D'Haena, K. Bertoldia, *Proc. Natl. Acad. Sci. USA* **2015**, *112*, 10863.
[101] W. Fan, C. Shan, H. Guo, J. Sang, R. Wang, R. Zheng, K. Sui, Z. Nie, *Sci. Adv.* **2019**, *5*, eaav7174.
[102] J. E. Huber, N. A. Fleck, M. F. Ashby, *Proc. R. Soc. A* **1997**, *453*, 2185.
[103] V. Khare, S. Sonkaria, G. Y. Lee, S. H. Ahn, W. S. Chu, *Int. J. Precis. Eng. Manuf. – Green Technol.* **2017**, *4*, 291.
[104] J. W. Boley, W. M. Van Rees, C. Lissandrello, M. N. Horenstein, R. L. Truby, A. Kotikian, J. A. Lewis, L. Mahadevan, *Proc. Natl. Acad. Sci. USA* **2019**, *116*, 20856.
[105] K. Senthil Kumar, P. Chen, H. Ren, *Research* **2019**, 3018568.
[106] S. Kyle, Z. M. Jessop, A. Al-Sabah, I. S. Whitaker, *Adv. Healthcare Mater.* **2017**, *6*, 1700264.
[107] D. Soltman, V. Subramanian, *Langmuir* **2008**, *24*, 2224.
[108] D. Ding, Z. Pan, D. Cuiuri, H. Li, S. van Duin, in *New Trends in 3D Printing*, IntechOpen, London **2016**, pp. 3–24.
[109] K. N. Al-Milaji, R. R. Secondo, T. N. Ng, N. Kinsey, H. Zhao, *Adv. Mater. Interfaces* **2018**, *5*, 1701561.
[110] G. Grau, J. Cen, H. Kang, R. Kitsomboonloha, W. J. Scheideler, V. Subramanian, *Flexible Printed Electron.* **2016**, *1*, 023002.
[111] N. J. Wilkinson, M. A. A. Smith, R. W. Kay, R. A. Harris, *Int. J. Adv. Des. Manuf. Technol.* **2019**, *105*, 4599.
[112] X. Wang, M. Jiang, Z. Zhou, J. Gou, D. Hui, *Composites, Part B* **2017**, *110*, 442.
[113] D. E. Schwartz, T. N. Ng, *IEEE Electron Device Lett.* **2013**, *34*, 271.
[114] B. W. An, K. Kim, H. Lee, S. Y. Kim, Y. Shim, D. Y. Lee, J. Y. Song, J. U. Park, *Adv. Mater.* **2015**, *27*, 4322.
[115] C. Ladd, J. H. So, J. Muth, M. D. Dickey, *Adv. Mater.* **2013**, *25*, 5081.
[116] M. A. Skylar-Scott, J. Mueller, C. W. Visser, J. A. Lewis, *Nature* **2019**, *575*, 330.
[117] J. R. Tumbleston, D. Shirvanyants, N. Ermoshkin, R. Janusziewicz, A. R. Johnson, D. Kelly, K. Chen, R. Pinschmidt, J. P. Rolland, A. Ermoshkin, E. T. Samulski, J. M. DeSimone, *Science* **2015**, *347*, 1349.

[118] A. Vyatskikh, S. Delalande, A. Kudo, X. Zhang, C. M. Portela, J. R. Greer, *Nat. Commun.* **2018**, *9*, 593.
[119] H. Kim, Z. Wu, N. Eedugurala, J. D. Azoulay, T. N. Ng, *ACS Appl. Mater. Interfaces* **2019**, *11*, 36880.
[120] T. N. Ng, D. E. Schwartz, P. Mei, S. Kor, J. Veres, P. Bröms, C. Karlsson, *Flexible Printed Electron.* **2016**, *1*, 015002.
[121] Z. Wu, Y. Zhai, W. Yao, N. Eedugurala, S. Zhang, L. Huang, X. Gu, J. D. Azoulay, T. N. Ng, *Adv. Funct. Mater.* **2018**, *28*, 1805738.
[122] Y. Zhai, J. Lee, Q. Hoang, D. Sievenpiper, H. Garudadri, T. N. Ng, *Flexible Printed Electron.* **2018**, *3*, 035006.
[123] K. Wang, U. Parekh, J. K. Ting, N. A. D. Yamamoto, J. Zhu, T. Costantini, A. C. Arias, B. P. Eliceiri, T. N. Ng, *Adv. Biosyst.* **2019**, *3*, 1900106.
[124] E. Saleh, F. Zhang, Y. He, J. Vaithilingam, J. L. Fernandez, R. Wildman, I. Ashcroft, R. Hague, P. Dickens, C. Tuck, *Adv. Mater. Technol.* **2017**, *2*, 1700134.
[125] Y. Yoshida, H. Wada, K. Izumi, S. Tokito, *Jpn. J. Appl. Phys.* **2017**, *56*, 05EA01.
[126] X. Guo, Y. Xu, S. Ogier, T. N. Ng, M. Caironi, A. Perinot, L. Li, J. Zhao, W. Tang, R. A. Sporea, A. Nejim, J. Carrabina, P. Cain, F. Yan, *IEEE Trans. Electron Devices* **2017**, *64*, 1906.
[127] T. N. Ng, D. E. Schwartz, P. Mei, B. Krusor, S. Kor, J. Veres, P. Bröms, T. Eriksson, Y. Wang, O. Hagel, C. Karlsson, *Sci. Rep.* **2015**, *5*, 13457.
[128] T. Kim, R. Trangkanukulkij, W. S. Kim, *Sci. Rep.* **2018**, *8*, 3805.
[129] S. Ready, G. Whiting, T. N. Ng, *NIP and Digital Fabrication Conf., 2014*, Vol. *4*, Society for Imaging Science and Technology, Springfield, VA, USA **2014**, pp. 120–123.
[130] K. Wang, U. Parekh, T. Pailla, H. Garudadri, V. Gilja, T. N. Ng, *Adv. Healthcare Mater.* **2017**, *6*, 1700552.
[131] N. Matsuhisa, D. Inoue, P. Zalar, H. Jin, Y. Matsuba, A. Itoh, T. Yokota, D. Hashizume, T. Someya, *Nat. Mater.* **2017**, *16*, 834.
[132] M. D. Dickey, *Adv. Mater.* **2017**, *29*, 1606425.
[133] J. Wang, G. Cai, S. Li, D. Gao, J. Xiong, P. S. Lee, *Adv. Mater.* **2018**, *30*, 1706157.
[134] S. H. Park, M. Kaur, D. Yun, W. S. Kim, *Langmuir* **2018**, *34*, 10897.
[135] K. Wang, L. Huang, N. Eedugurala, S. Zhang, M. A. Sabuj, N. Rai, X. Gu, J. D. Azoulay, T. N. Ng, *Adv. Energy Mater.* **2019**, *9*, 1902806.
[136] S. H. Park, R. Su, J. Jeong, S. Z. Guo, K. Qiu, D. Joung, F. Meng, M. C. McAlpine, *Adv. Mater.* **2018**, *30*, 1803980.
[137] Z. Wu, Y. Zhai, H. Kim, J. D. Azoulay, T. N. Ng, *Acc. Chem. Res.* **2018**, *51*, 3144.
[138] B. E. Kelly, I. Bhattacharya, H. Heidari, M. Shusteff, C. M. Spadaccini, H. K. Taylor, *Science* **2019**, *363*, 1075.
[139] P. Wang, D. B. Berry, Z. Song, W. Kiratitanaporn, J. Schimelman, A. Moran, F. He, B. Xi, S. Cai, S. Chen, *Adv. Funct. Mater.* **2020**, *30*, 1910391.
[140] S. Liu, M. C. Yuen, R. Kramer-Bottiglio, *Flexible Printed Electron.* **2019**, *4*, 015004.
[141] M. Kaur, W. S. Kim, *Adv. Intell. Syst.* **2019**, *1*, 1900019.
[142] A. M. Abdullah, X. Li, P. V. Braun, J. A. Rogers, K. J. Hsia, *Adv. Funct. Mater.* **2020**, *30*, 1909888.
[143] A. Rafsanjani, L. Jin, B. Deng, K. Bertoldi, *Proc. Natl. Acad. Sci. USA* **2019**, *116*, 8200.
[144] C. Wang, C. Wang, Z. Huang, S. Xu, *Adv. Mater.* **2018**, *30*, 1801368.
[145] H. Yuk, T. Zhang, G. A. Parada, X. Liu, X. Zhao, *Nat. Commun.* **2016**, *7*, 12028.
[146] D. Wirthl, R. Pichler, M. Drack, G. Kettlguber, R. Moser, R. Gerstmayr, F. Hartmann, E. Bradt, R. Kaltseis, C. M. Siket, S. E. Schausberger, S. Hild, S. Bauer, M. Kaltenbrunner, *Sci. Adv.* **2017**, *3*, e1700053.
[147] Y. Zhao, A. Kim, G. Wan, B. C. K. Tee, *Nano Convergence* **2019**, *6*, 25.
[148] S. Ready, F. Endicott, G. Whiting, T. N. Ng, E. Chow, J.-P. Lu. in *NIP and Digital Fabrication Conf. 2013*, Society for Imaging Science and Technology, Springfield, VA, USA **2013**, pp. 9–12.
[149] G. L. Whiting, D. E. Schwartz, T. N. Ng, B. S. Krusor, R. Krivacic, A. Pierre, A. C. Arias, M. Harting, D. van Buren, K. L. Short, *Flexible Printed Electron.* **2017**, *2*, 034002.
[150] Z. Suo, E. Y. Ma, H. Gleskova, S. Wagner, *Appl. Phys. Lett.* **1999**, *74*, 1177.
[151] P. Mei, B. Krusor, D. E. Schwartz, T. N. Ng, G. Daniel, S. Ready, G. L. Whiting, *IEEE Sens. J.* **2017**, *17*, 7114.
[152] R. J. M. Wolfs, F. P. Bos, E. C. F. Van Strien, T. A. M. Salet, in *High Tech Concrete: Where Technology and Engineering Meet – Proc. of the 2017 fib Symp.* (Eds: D. A. Hordijk, M. Luković), Springer, New York **2017**, pp. 2474–2483.
[153] S. E. Root, C. W. Carpenter, L. V. Kayser, D. Rodriquez, D. M. Davies, S. Wang, S. T. M. Tan, Y. S. Meng, D. J. Lipomi, *ACS Omega* **2018**, *3*, 662.
[154] N. Besse, S. Rosset, J. J. Zarate, H. Shea, *Adv. Mater. Technol.* **2017**, *2*, 1700102.
[155] L. Liu, B. Geng, S. M. Sayed, B. P. Lin, P. Keller, X. Q. Zhang, Y. Sun, H. Yang, *Chem. Commun.* **2017**, *53*, 1844.
[156] C. M. Yakacki, M. Saed, D. P. Nair, T. Gong, S. M. Reed, C. N. Bowman, *RSC Adv.* **2015**, *5*, 18997.
[157] M. O. Saed, A. H. Torbati, D. P. Nair, C. M. Yakacki, *J. Visualized Exp.* **2016**, *2016*, 1.
[158] J. J. Zárate, H. Shea, *IEEE Trans. Haptics* **2017**, *10*, 106.
[159] G. Cai, J. H. Ciou, Y. Liu, Y. Jiang, P. S. Lee, *Sci. Adv.* **2019**, *5*, eaaw7956.
[160] U. Kim, J. Kang, C. Lee, H. Y. Kwon, S. Hwang, H. Moon, J. C. Koo, J. D.o Nam, B. H. Hong, J. B. Choi, H. R. Choi, *Nanotechnology* **2013**, *24*, 145501.
[161] F. Chen, D. Yuan Lei, *Sci. Rep.* **2015**, *5*, 11552.
[162] G. Park, S. Kang, H. Lee, W. Choi, *Sci. Rep.* **2017**, *7*, 41000.
[163] S. W. Ula, N. A. Traugutt, R. H. Volpe, R. R. Patel, K. Yu, C. M. Yakacki, *Liq. Cryst. Rev.* **2018**, *6*, 78.

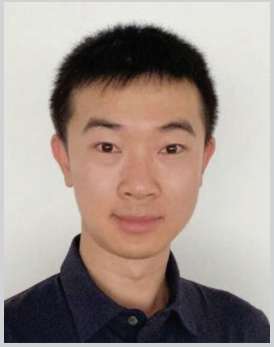

**Yichen Zhai** received his B.S. in microelectronics from Changchun University of Science and Technology and his M.S. in electrical engineering from Stevens Institute of Technology. He is a Ph.D. candidate at University of California San Diego (UCSD). His research interests are development of 3D printers and printing electronic devices.

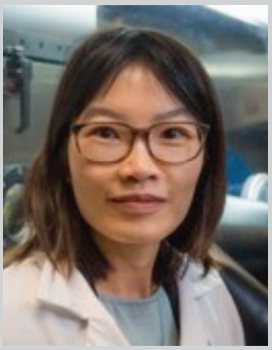

**Tse Nga Ng** is an associate professor in the Department of Electrical and Computer Engineering at UCSD. Her research focuses on materials and devices in flexible electronics, as well as novel fabrication techniques toward additive manufacturing. More details can be found on her website: http://flexible-electronics.ucsd.edu/. Prior to UCSD, she was a research scientist at Palo Alto Research Center, a Xerox Company. She received her Ph.D. in physical chemistry under the mentorship of Prof. John Marohn at Cornell University.